A&A manuscript no.
(will be inserted by hand later)

Your thesaurus codes are:
06 (08.02.1; 08.03.2; 08.05.3; 08.19.4; 9.19.2)

ASTRONOMY AND ASTROPHYSICS

The evolution of main sequence star + white dwarf binary systems towards Type Ia supernovae

N. Langer[1], A. Deutschmann[1], S. Wellstein[1] and P. Höflich[2]

[1] Institut für Physik, Universität Potsdam, Am Neuen Palais 10, D–14415 Potsdam, Germany
[2] Department of Astronomy, University of Texas, Austin, TX 78712, USA

Received ; accepted ,

Abstract. Close binaries consisting of a main sequence star and a white dwarf are considered as candidates for Type Ia supernova progenitors. We present selfconsistent calculations of the time dependence of the structure of the main sequence star, the mass transfer rate, and the orbit by means of a binary stellar evolution program. We obtain, for the first time, a complete picture of the time evolution of the mass transfer rate in such systems. We find a long switch-on phase of the mass transfer, about 10^6 yr, during which nova outbursts should persist in all systems. Furthermore, we find that the white dwarfs can reach the Chandrasekhar mass only during the decline phase of the mass transfer, which may have consequences for the critical accretion rate for stationary nuclear burning on the white dwarf surface. In contrast to results based on simple estimates of the mass transfer rate in systems of the considered type, our results can not exclude the possibility that even systems with rather small initial white dwarf masses ($\sim 0.7\,\mathrm{M}_\odot$) may produce Type Ia supernovae, which then might originate from very rapidly rotating white dwarfs.

We present results for two different metallicities, Z=0.02 and Z=0.001. We find that for systems with low metallicity, the mass transfer rates are on average five times larger than in comparable system at solar metallicity. This leads to a systematic shift of the supernova Ia progenitor population. Firstly, while for Z=0.02 donor star initial masses are restricted to the the range $1.6\,\mathrm{M}_\odot...2.3\,\mathrm{M}_\odot$, they are in the interval $1.4\,\mathrm{M}_\odot...1.8\,\mathrm{M}_\odot$ at low Z. Secondly, the initial white dwarf masses need, on average, to be larger by $0.2\,\mathrm{M}_\odot$ at low Z in order to obtain a Chandrasekhar mass white dwarf. This metallicity dependences have very little effect on the progenitor life times, but may be responsible for a drop of the Type Ia supernova rate for low metallicity, and may introduce a Z-dependence in the properties of supernovae which stem from close main sequence star + white dwarf systems.

We estimate the X-ray luminosities of the computed systems, and investigate their donor star and orbital properties. We find the donor stars to be underluminous by up to one order of magnitude, and more compact than normal main sequence stars. In general, our systems correspond well to observed close binary supersoft X-ray sources. We further derive the chemical and kinematical properties of the stellar remnants of our systems after the explosion of the white dwarf, which may serve as a test of the viability of the considered Type Ia supernova scenario.

Send offprint requests to: N. Langer (email: `ntl@astro.physik.uni-potsdam.de`)

1. Introduction

During the last years, the refinement of supernova observations, e.g., the routine detection of supernovae at large redshifts, has made them a powerful tool to probe cosmology. It allowed to determine the Hubble constant with unprecedented accuracy (Riess et al. 1995, Hamuy et al. 1996; see also Höflich & Khokhlov 1996). Even more exciting, recent results (e.g., Riess et al. 1999, Perlmutter et al. 1999) are consistent with a low matter density in the Universe and, intriguingly, hints for a positive cosmological constant. These findings are based on empirical brightness-decline relations which are calibrated locally. This leaves potential systematic effects of supernova Ia properties with redshift as major concern. To this end, it would be desirable to obtain an estimate of such effects from theoretical models of supernova Ia progenitor systems.

However, despite considerable efforts during the last decades, the exact nature of supernova Ia progenitors is still unclear. On observational and theoretical grounds, it is generally agreed that Type Ia supernovae result from the thermonuclear disruption of a CO white dwarf (e.g., Woosley & Weaver 1986, Wheeler 1996, Nomoto et al. 1997, Branch 1998). Since isolated white dwarfs cool, a close binary component which transfers mass to the white dwarf is a prerequisite to obtain a Type Ia supernova.

Various binary evolution scenarios leading to exploding CO white dwarfs have been proposed and investigated, but hitherto it is unclear which of them is preferred in nature (cf. Branch 1988, Livio 1999).

In this paper, we study the evolution of close binary systems consisting of a carbon-oxygen white dwarf and a main sequence star, which was repeatedly proposed as promising supernova Ia progenitor scenario (cf. Nomoto & Sugimoto 1977, Li & van den Heuvel 1997, Kato & Hachisu 1999, Hachisu et al. 1999). In these systems, the carbon-oxygen white dwarfs are the remainders of stars with an initial mass below $\approx 10\,\mathrm{M}_\odot$ which have lost their H/He-rich envelope, with CO cores of $\approx 0.6 ... 1.2\,\mathrm{M}_\odot$. If accretion is sufficiently fast the accreted hydrogen may burn to helium and, subsequently, to CO on the surface of the white dwarf, and its mass grows close to the Chandrasekhar mass.

The binary evolution leading to close white dwarf + main sequence star systems is not yet well understood (cf., Livio 1996). However, we know a large number ($\sim 10^3$) of close white dwarf + main sequence star systems as Cataclysmic Variables (Ritter & Kolb 1998), most of which do not evolve into Type Ia supernovae since they undergo nova outbursts which may prevent a secular increase of the white dwarf mass (e.g., Kovetz & Prialnik 1997). The idea that also the slightly more massive white dwarf + main sequence star systems studied here occur in nature is supported by population synthesis studies, which predict their birth rate to be comparable, within an order of magnitude, to the observed rate of Ia supernovae (e.g., de Kool & Ritter 1993, Rappaport et al, 1994). It is further supported through the discovery of the so called supersoft X-ray sources (Greiner et al. 1991, Kahabka & van den Heuvel 1997), which may represent the observational counterparts of the binary systems studied here theoretically.

We investigate the properties of close main sequence star-white dwarf systems at two different metallicities. As we derive the detailed time-dependence of the accretion rate, our work is relevant for the understanding of individual supernovae and supersoft X-ray binaries, for the change of their average properties with metallicity, and for the dependence of the rate of Ia supernovae with metallicity. We introduce our computational method in Section 2, and present our results for the mass transfer rate and resulting maximum white dwarf masses in Section 3. In Section 4, we discuss the evolution of the white dwarf spin, of the binary orbit and of the main sequence stars. In Section 5, we compare our results with observations of supersoft X-ray sources and derive clues which may help to identify the remaining main sequence star in a supernova Ia remnant. Our conclusions are given in Section 6.

2. Computational method and physical assumptions

The numerical models presented in this work are computed with a binary stellar evolution code developed by Braun (1997) on the basis of a single star code (Langer 1998, and references therein). It is a 1-dimensional implicit Lagrangian code which solves the hydrodynamic form of the stellar structure and evolution equations (Kippenhahn & Weigert 1990). The evolution of two stars and, in case of mass transfer, the evolution of the mass transfer rate and of the orbital separation are computed simultaneously through an implicit coupling scheme (see also Wellstein & Langer 1999, Wellstein et al. 1999), using the Roche-approximation in the formulation of Eggleton (1983). To compute the mass transfer rate, we use the description of Ritter (1988). The stellar models are computed using OPAL opacities (Iglesias & Rogers 1996) and extended nuclear networks including the pp I, II, and III chains, the four CNO-cycles, and the NeNa- and MgAl-cycles (cf. Arnould et al. 1999).

2.1. The mass accretion rate of the white dwarf

In order to compute the evolution of close main sequence star-white dwarf pairs, we invoke the following assumptions. In the computation of the binary system the white dwarf is approximated as a point mass (however, cf. Section 2.3), while the main sequence star is resolved with typically 1000 grid points. The systems are started at time t:=0 with a zero age main sequence star of mass $M_{1,\mathrm{i}}$ and an arbitrary white dwarf mass $M_{\mathrm{WD,i}}$ at an arbitrary orbital separation d_i. For most models, we use $M_{\mathrm{WD,i}} = 0.8\,\mathrm{M}_\odot$ or $1.0\,\mathrm{M}_\odot$. For d_i we consider only values which lead to mass transfer during the core hydrogen burning phase of the main sequence star, i.e. so called Case A mass transfer.

The mass of the white dwarf (the point mass) was allowed to vary in accordance with critical mass transfer rates which were taken from the literature as follows. For mass transfer rates $\dot{M} \geq \dot{M}_\mathrm{H}(M_\mathrm{WD})$ and $\dot{M} \geq \dot{M}_\mathrm{He}(M_\mathrm{WD})$, we allowed the white dwarf mass to increase. Here, $\dot{M}_\mathrm{H}$ and $\dot{M}_\mathrm{He}$ are the critical accretion rates above which H- or He-burning proceeds such that violent nova flashes and consequent mass ejection from the white dwarf are avoided. We adopted $\dot{M}_\mathrm{He} = 10^{-8}\ \mathrm{M}_\odot\ \mathrm{yr}^{-1}$ for models with a metallicity of $Z = 2\%$, and $4\,10^{-8}\ \mathrm{M}_\odot\ \mathrm{yr}^{-1}$ for $Z = 0.001$ (Fujimoto 1982, Nomoto & Kondo 1991). For $\dot{M}_\mathrm{H}$ we relied on Figure 5 of Kahabka & van den Heuvel (1997). For $\dot{M}_\mathrm{He} > \dot{M} > \dot{M}_\mathrm{H}$ we assumed the white dwarf mass to grow as well, but by accumulating a degenerate thick helium layer. For $\dot{M} \leq \dot{M}_\mathrm{Edd} := L_\mathrm{Edd}/\varepsilon$ and $\dot{M} \leq \dot{M}_\mathrm{RG}$, we assume $\dot{M}_\mathrm{WD} = \dot{M}$. Here, $\dot{M}_\mathrm{RG}$ is the critical accretion rate above which the white dwarf is assumed to expand to red giant dimensions (Nomoto & Kondo 1991), and

$$L_{\rm Edd} = \frac{4\pi c G M_{\rm WD}}{0.2 * (1+X)} \quad (1)$$

is the Eddington luminosity of the white dwarf, using $0.2 * (1 + X)$ as the opacity coefficient due to electron scattering with X being the hydrogen mass fraction. The quantity $\varepsilon = 7\,10^{18}\,{\rm erg\,g^{-1}}$ gives the approximate amount of energy obtained per gram of hydrogen burnt into helium or carbon/oxygen. For larger mass transfer rates we assume that the white dwarf has a wind which carries the excess mass away (Hachisu et al. 1996). We stop our calculations for models with $\dot{M}_{\rm wind} > 3\dot{M}_{\rm Edd}$.

Our assumptions concerning the critical accretion rates are similar to those of Li & van den Heuvel (1997). However, we deviate from them by adopting a maximum possible wind mass loss rate of $\dot{M}_{\rm wind} > 3\dot{M}_{\rm Edd} \simeq 5\,10^{-7}\,{\rm M_\odot\ yr^{-1}}$, rather than $10^{-4}\,{\rm M_\odot\ yr^{-1}}$. We do so since already for $\dot{M} = 2M_{\rm Edd}$ the wind momentum $\dot{M}_{\rm wind} v_\infty = \dot{M}_{\rm Edd} v_\infty$ is of the order of the photon momentum $L_{\rm Edd}/c$. Here, v_∞ is the terminal wind velocity. More specific, $\dot{M}_{\rm wind} = \dot{M}_{\rm Edd}$ implies

$$\frac{\dot{M}_{\rm wind} v_\infty}{L/c} = \frac{v_\infty c}{\varepsilon} \quad (2)$$

which, for

$$v_\infty \simeq v_{\rm escape} = \sqrt{\frac{2GM_{\rm WD}}{R_{\rm WD}}} \quad (3)$$

(Lamers & Cassinelli 1999), is of order unity. I.e., we prefer to limit our wind mass loss rate such that the wind momentum flux does not exceed few times the photon momentum flux. The consequences of this assumption, which also deviates from assumptions on wind mass loss rates in previous studies (cf. Hachisu et al. 1996, Kobayashi et al. 1998) are discussed in Section 3.4. Self-excited wind as proposed by King & van Teeseling (1998) are not considered here.

Other than Li & van den Heuvel (1997), we do not allow for the possibility of the partial mass ejection in case of weak shell flashes, as we think that the current uncertainties (cf. Prialnik & Kovetz 1995) my not make such sophistication worthwhile but rather complicate the understanding of the obtained results. Our value of $\dot{M}_{\rm H} = 10^{-8}\,{\rm M_\odot\ yr^{-1}}$ for $Z = 2\%$ is in agreement with the general conclusion of Prialnik & Kovetz that $\dot{M} \gtrsim 10^{-8}\,{\rm M_\odot\ yr^{-1}}$ leads to growing white dwarf masses. However, we investigate the effect of an increase of this threshold value by one order of magnitude, as outlined in Section 3.4.

2.2. Further white dwarf properties

Basic properties of the white dwarf are estimated as follows: Its radius $R_{\rm WD}$ is given by the mass-radius relation

$$R_{\rm WD} = f M_{\rm WD}^{-1/3} \quad (4)$$

with $f = \frac{2}{G}(\frac{3}{8\pi})^{4/3} h^2 / \left(2^{1/3}\mu_e^{5/3} m_p^{5/3} m_e\right) \simeq 9.03\,10^{19}\,{\rm cm\,g^{1/3}}$ (Kippenhahn & Weigert 1990; see also Nauenberg 1972, Provencal et al. 1998).

We assume that the radiation from the white dwarf can be approximated by a Black Body with an effective temperature

$$T_{\rm WD} = \frac{\varepsilon \dot{M}_{\rm WD}}{4\pi R_{\rm WD}^2 \sigma}, \quad (5)$$

with $\sigma = 5.67\,10^{-5}\,{\rm erg\,s^{-1}\,cm^{-2}\,K^{-4}}$ being the Stefan-Boltzmann constant.

We estimate the white dwarf's angular momentum and rotation frequency by assuming it to be zero initially, and that the specific angular momentum of the accreted matter is $j = v_{\rm Kepler} R_{\rm WD}$, with $v_{\rm Kepler} = \sqrt{GM_{\rm WD}/R_{\rm WD}}$. The equation for the accumulated angular momentum

$$J := \int_{t'=0}^{t} = \dot{M}_{\rm WD} j\,dt', \quad (6)$$

yields

$$J = \frac{3}{4}\sqrt{Gf}\left(M_{\rm WD}^{4/3} - M_{\rm WD,i}^{4/3}\right). \quad (7)$$

Assuming then rigid rotation for the white dwarf interior (cf. Kippenhahn 1974) we can estimate its angular velocity as

$$\omega = \frac{J}{k^2 M_{\rm WD} R_{\rm WD}^2} \quad (8)$$

where k is the dimensionless radius of gyration . The ratio $\Omega = \omega/\omega_{\rm Kepler}$ becomes

$$\Omega = \frac{3}{4k^2}\left(1 - \left(\frac{M_{\rm WD,i}}{M_{\rm WD}}\right)^{4/3}\right) \quad (9)$$

(cf. Papaloizou & Pringle 1978, Livio & Pringle 1998). The implications of this relation are discussed in Section 3.3.

2.3. Single star evolution

We have constructed stellar model sequences for two metallicities, $Z = 0.02$ and $Z = 0.001$. The initial helium mass fraction is computed as $Y = Y_{\rm pm} + (dY/dZ)Z$, using $Y_{\rm pm} = 0.24$ as primordial helium mass fraction and $dY/dZ = 2$. The resulting values are $Y = 0.280$ and $Y = 0.242$ for the high and low metallicity considered here, respectively. The relative abundances of the metals are chosen according to the solar system abundances (Grevesse & Sauval 1998). We have computed all models with extended convective cores ("overshooting") by 0.2 pressure scale heights ($\alpha_{\rm over} = 0.2$). The resulting tracks in the HR diagram are very similar to those of Schaller et al. (1992), that of our $Z = 0.02$ models for $2\,{\rm M_\odot}$ and $1.7\,{\rm M_\odot}$ and of our $2\,{\rm M_\odot}$ sequence at $Z = 0.001$ — the only three sequences which we can directly compare — are virtually identical.

Figs. 1 and 2 show the time evolution of the radii during core hydrogen burning for our single star models at

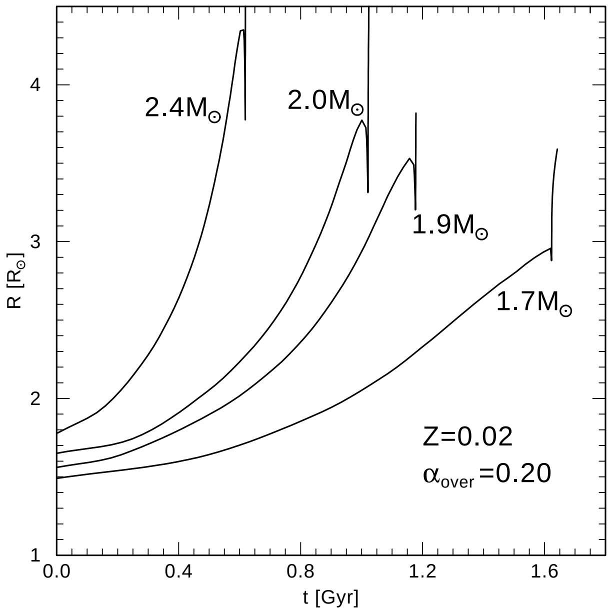

Fig. 1. Evolution of the stellar radius as a function of time for single stars of about solar metallicity (Z=0.02) in the mass range from 1.7 to 2.4 $M_\odot$ computed with convective core overshooting ($\alpha_{\rm over} = 0.2$), from the zero age main sequence until shortly after core hydrogen exhaustion.

Table 1. Comparison of surface properties and of the Kelvin-Helmholtz time scale $\tau_{\rm KH,TAMS} = GM^2/(2RL)$ for models of $2\,M_\odot$ sequences computed with metallicities of $Z = 0.02$ and $Z = 0.001$, at the zero age main sequence (ZAMS) and the terminal age main sequence (TAMS)

	$Z = 0.02$	$Z = 0.001$
$L_{\rm ZAMS}$	15.9 $L_\odot$	26.3 $L_\odot$
$T_{\rm eff,ZAMS}$	9158 K	12474 K
$R_{\rm ZAMS}$	1.60 $R_\odot$	1.11 $R_\odot$
$\tau_{\rm KH,ZAMS}$	2.5Myr	2.2Myr
$L_{\rm TAMS}$	22.3 $L_\odot$	56.1 $L_\odot$
$T_{\rm eff,TAMS}$	6600 K	10452 K
$R_{\rm TAMS}$	3.65 $R_\odot$	2.31 $R_\odot$
$\tau_{\rm KH,TAMS}$	0.75Myr	0.48Myr

the two metallicities considered in this work, for the mass range which is relevant in the context of this paper. During core hydrogen burning, the radii increase by factors 2.0...2.5 and 1.7...2.3 for the higher and lower considered metallicity, respectively, with larger values corresponding to larger masses.

The radii of the metal poor stars are nearly a factor of 2 smaller than those of stars with a comparable mass and evolutionary stage at $Z = 0.02$. This has consequences for the binary evolution models discussed below, i.e., the orbital periods in Case A systems are much smaller for smaller metallicity. Furthermore, the metal poor main sequence stars are hotter and more luminous compared to stars of the same mass at $Z = 0.02$. This is in agreement with previous models of stars of comparable masses and

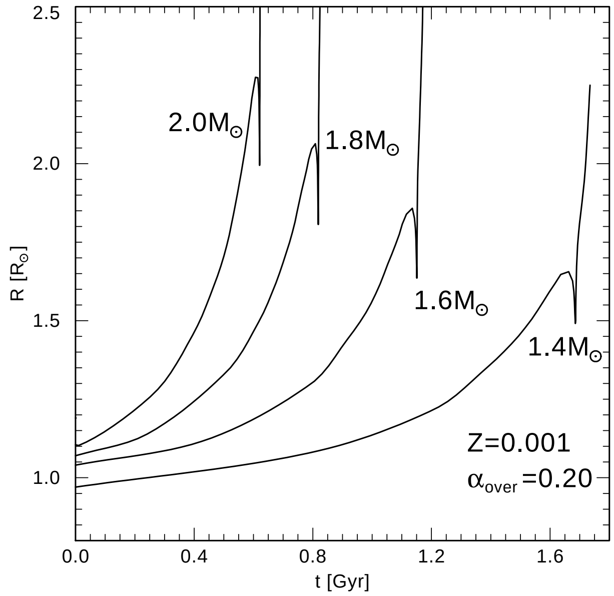

Fig. 2. Same as Figure 1, but for low metallicity stars (Z=0.001) in the mass range 1.4 to 2 $M_\odot$.

metallicities (e.g., Schaller et al. 1992). Table 1 gives the quantitative details of models from our $2\,M_\odot$ sequences at $Z = 0.02$ and $Z = 0.001$ at the beginning and at the end of core hydrogen burning. Although the models at lower metallicities are more compact, they are also more luminous than the metal richer models, with the consequence of a shorter Kelvin-Helmholtz time scale. This has consequences for the mass transfer rates, as discussed in the next section.

2.4. Binary evolution: examples

To illustrate our approach, we consider our System No. 6. Initially, it consists of a $2\,M_\odot$ zero age main sequence star and a $1\,M_\odot$ white dwarf (treated as point mass) in a circular orbit with a separation of $d_{\rm i} = 7.19\,R_\odot$. According to Kepler's third law, the initial period $P_{\rm i}$ is

$$P_{\rm i} = \frac{2\pi}{\sqrt{G}} \sqrt{\frac{d_{\rm i}^3}{M_{\rm MS,i} + M_{\rm WD,i}}} \qquad (10)$$

i.e., $P_{\rm i} = 1.29$ d in this case. With this initial set-up, we skip the previous evolution of the system, i.e. the evolution of the white dwarf progenitor and the common envelope and spiral-in phase which brought the two stars close together.

We set the time $t = 0$ at core hydrogen ignition of our main sequence star. In principle, this neglects the duration of the previous evolution of the system, i.e. the evolutionary time of the white dwarf progenitor. However, as we shall see below we deal with rather high initial white dwarf masses, i.e. relatively massive white dwarf progenitor stars ($\gtrsim 5\,M_\odot$). Therefore, as the white dwarf starts to accrete at a system age of the order of the evolutionary

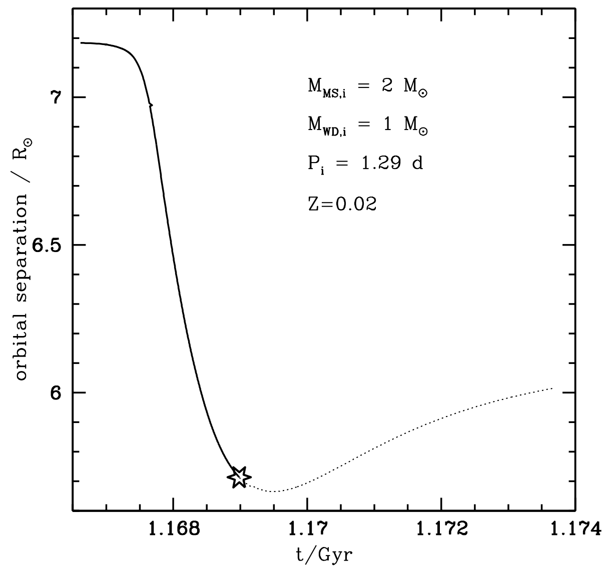

Fig. 3. Evolution of the orbital period as function of time for System No. 6 (cf. Table 1). The curve starts at the onset of mass transfer at $t \simeq 1.166$ Gyr. At $t \simeq 1.169$, the white dwarf mass has grown to $1.4\,\mathrm{M}_\odot$; this time is marked by an asterisk on the curve. The dashed part of the curve shows the continuation of the orbital period evolution assuming that the white dwarf does not perform a supernova explosion.

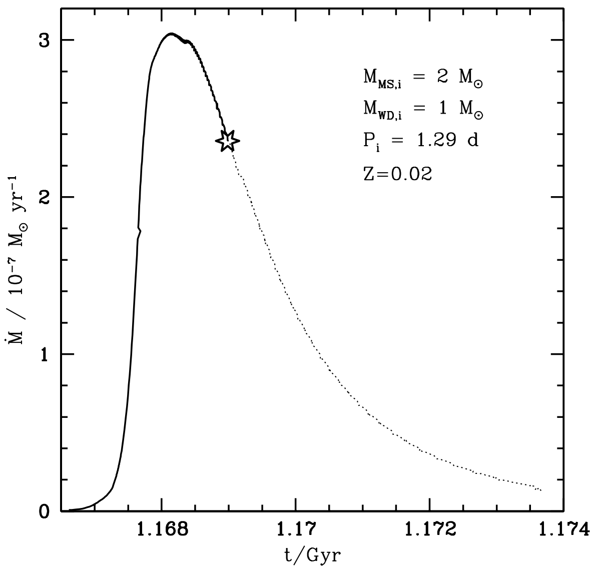

Fig. 4. Evolution of the mass transfer rate as function of time for System No. 6 (cf. Table 1). The curve starts at the onset of mass transfer at $t \simeq 1.166$ Gyr. At $t \simeq 1.169$, the white dwarf mass has grown to $1.4\,\mathrm{M}_\odot$; this time is marked by an asterisk on the curve. The dashed part of the curve shows the continuation of the mass transfer rate evolution assuming that the white dwarf does not perform a supernova explosion.

time scale of the donor star ($1.4...2.4\,\mathrm{M}_\odot$; see below) the so defined time yields a good estimate for the age of the systems at the time of the supernova explosion (cf. Umeda et al. 1999).

In our System No. 6, mass transfer starts at $t \simeq 1.166$ Gyr, at a central hydrogen mass fraction of the main sequence star of $X_\mathrm{c} \simeq 0.17$. The radius of the star has then grown from $R_\mathrm{i} \simeq 1.60\,\mathrm{R}_\odot$ at the ZAMS to $R \simeq 3.16\,\mathrm{R}_\odot$, as we use Eggleton's (1983) approximation for the Roche radius of the main sequence star

$$R_\mathrm{L} = d\frac{0.49q^{2/3}}{0.6q^{2/3}\ln(1+q^{1/3})} \tag{11}$$

with $q := M_\mathrm{MS}/M_\mathrm{WD}$.

During the initial phase of the mass transfer evolution, the mass transfer rate $\dot{M}$ is still smaller than $\dot{M}_\mathrm{H}$ (cf. Section 2.1), and the white dwarf mass can not increase. Instead, all accreted mass is assumed to be lost in nova outbursts, carrying away the specific orbital angular momentum of the white dwarf, leading to a decrease of the orbital separation (cf. Podsiadlowski et al. 1992). The amount of mass lost during this phase, and consequently the change of the orbital parameters, is quite insignificant in most cases. E.g., in our example $0.003\,\mathrm{M}_\odot$ are transferred and lost in nova outbursts. However, we emphasize that the time scale of this first phase may be non-negligible, as it may be of the same order of magnitude as the major mass accretion phase (cf. Section 3).

When the mass transfer rate exceeds the critical rates for hydrogen and helium burning (Section 2.1), we allow the white dwarf mass to grow. As angular momentum conservation again leads to a shrinkage of the orbit as long as $M_\mathrm{MS} > M_\mathrm{WD}$, the mass transfer is thermally unstable. Since the mass-radius exponents of our main sequence stars are positive, i.e., mass loss leads to smaller radii (Ritter 1996), the mass transfer is stabilized due to the thermal disequilibrium of the main sequence star, and the resulting mass transfer rates are of the order of magnitude of

$$\dot{M} \simeq (M_\mathrm{MS,i} - M_\mathrm{WD,i})/\tau_\mathrm{KH} \tag{12}$$

(e.g., Rappaport et al. 1994; however, see Sect. 3.1).

Fig. 3 shows the evolution of the orbital separation with time for System No. 6 throughout the phase of the thermally unstable mass transfer. Within our approximations, the white dwarf mass reaches $1.4\,\mathrm{M}_\odot$ at $t \simeq 1.169$ Gyr. Although it is likely that the white dwarf would explode roughly at this point (see below), we follow the further evolution of the system ignoring this, for several reasons. Most important, the continued evolution allows us to estimate how changes in our basic assumptions might affect the fate of the white dwarf. E.g., since it appears to be undisputed that the white dwarf mass can grow for mass transfer rates $\dot{M} \gtrsim 10^{-7}\ \mathrm{M}_\odot\ \mathrm{yr}^{-1}$ (Nomoto & Kondo 1991, Prialnik & Kovetz 1995, Kahabka & van den Heuvel 1997), we define $M_7 := \int \dot{M}_7 dt$ with

$$\dot{M}_7 = \begin{cases} 0 & \text{for } \dot{M} < 10^{-7}\ \mathrm{M}_\odot\ \mathrm{yr}^{-1} \\ \dot{M}_\mathrm{WD} & \text{for } \dot{M} \geq 10^{-7}\ \mathrm{M}_\odot\ \mathrm{yr}^{-1} \end{cases} . \tag{13}$$

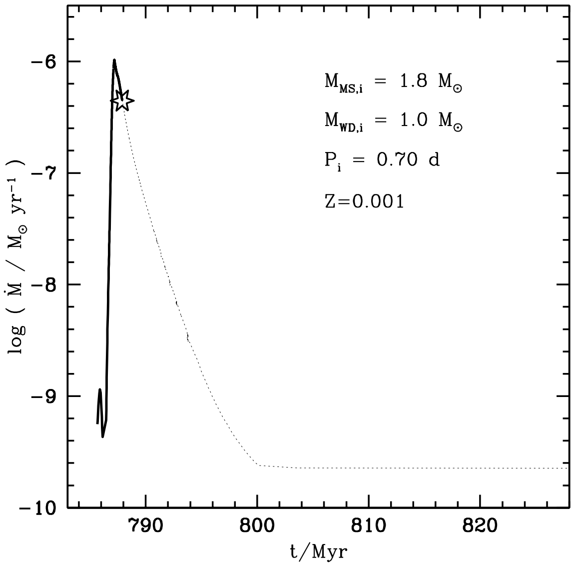

Fig. 5. Evolution of the mass transfer rate as function of time for System No. 61 (cf. Fig. 8).

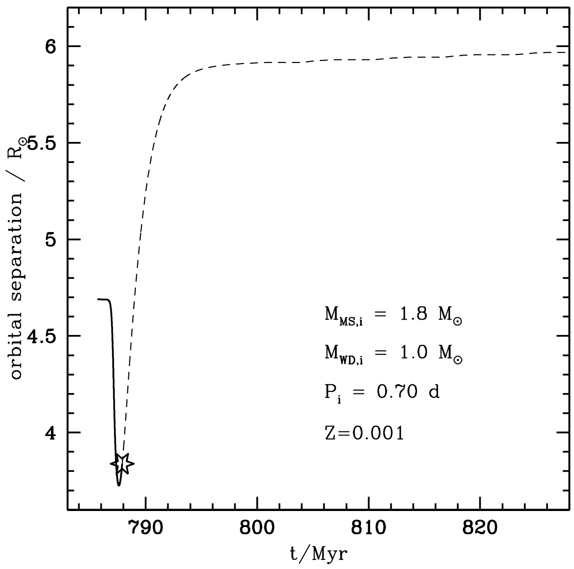

Fig. 6. Evolution of the orbital separation as function of time for System No. 61.

I.e., M_7 gives the amount of mass by which the white dwarf grows at accretion rates above 10^{-7} $M_\odot$ yr^{-1}, including the continued evolution beyond $M_{WD} = 1.4\,M_\odot$.

For System No. 6, the point mass has grown to $1.75\,M_\odot$ by the time the mass transfer rate falls below the critical rate ($\sim 10^{-8}$ $M_\odot$ yr^{-1}). The quantity M_7 in this system is $M_7 = 0.60\,M_\odot$, which means that were the critical accretion rate as high as 10^{-7} $M_\odot$ yr^{-1}, the point mass would still have grown to $1.60\,M_\odot$. This can be understood from Fig. 4, which shows the mass transfer rate as function of time for System No. 6. It can be seen that the mass transfer rate remains above 10^{-7} $M_\odot$ yr^{-1} for several million years after the potential supernova explosion.

Note that this estimate is not fully self-consistent. I.e., were all the accreted mass lost through nova outbursts as long as the mass transfer rate were below 10^{-7} $M_\odot$ yr^{-1}, the orbital evolution would differ from that of our model. However, as the mass loss from the white dwarf would keep the mass ratio $q := M_{MS}/M_{WD}$ above one for a longer time, the orbit would keep shrinking for a longer time, which would keep the mass transfer rate higher than in our model (cf. Section 3.1). Thus, the value of M_7 which we derive is in fact a lower limit to the mass which is transfered at rates above 10^{-7} $M_\odot$ yr^{-1}.

Comparing Figs. 3 & 4 shows, that the mass transfer rate drops to small values only several million years after the minimum orbital separation is achieved. The reason is that at the time of minimum separation the main sequence star is still more compact than its thermal equilibrium configuration. I.e., even though the orbit does not shrink any more, the main sequence star expands towards its thermal equilibrium radius and drives further mass transfer thereby.

In Figs. 5 and 6 we show the long-term evolution of the mass transfer rate and of the orbital period for another system, No. 61, initially consisting of a low metallicity $1.8\,M_\odot$ main sequence star and a $1\,M_\odot$ white dwarf orbiting with a period of 0.70 d. One can see the thermally unstable mass transfer phase lasting for several million years, beyond which mass transfer continues only on the nuclear time scale of the main sequence star, i.e., several 10^9 yr. Consequently, the mass transfer rate drops to some 10^{-10} $M_\odot$ yr^{-1}. The system then resembles a Cataclysmic Variable, evolving on a time scale of $10^9 ... 10^{10}$ yr. Note that in CVs, this time scale may become shorter due to angular momentum loss through magnetic braking (Verbunt & Zwaan 1981) which is ignored in the present study. Magnetic braking is not relevant for the supernova Ia progenitor evolution for two reasons. First, the time scale of the thermally unstable mass transfer is only of the order of several million years, which is too short to allow a significant amount of angular momentum loss through this mechanism. Second, our main sequence stars do develop convective envelopes only in the final phase of the thermally unstable mass transfer phase. I.e., most of the time they have radiative envelopes and thus supposedly no magnetic wind. For the study of the long term evolution of those systems which fail to bring the white dwarf to explode as a supernova, magnetic braking might be relevant. This is, however, beyond the scope of the present investigation.

Table 2. Key properties of interacting main sequence star + white dwarf systems with $Z = 0.02$. The columns have the following meanings. (1) system number, (2) main sequence star initial mass, (3) white dwarf initial mass, (4) initial orbital period, (5) minimum period, (6) maximum possible CO-mass (see text), (7) main sequence star mass when $M_{\rm WD} = 1.4\,{\rm M}_{\odot}$, (8) total mass loss due to winds (9) see Eq. 13, (10) maximum mass transfer rate (11) maximum X-ray luminosity of the white dwarf (12) core hydrogen mass fraction of main sequence star at onset of mass transfer (13) system age when $M_{\rm WD} = 1.4\,{\rm M}_{\odot}$

Nr.	$M_{\rm MS,i}$ ${\rm M}_{\odot}$	$M_{\rm WD,i}$ ${\rm M}_{\odot}$	$P_{\rm i}$ d	$P_{\rm min}$ d	$M_{\rm CO}$ ${\rm M}_{\odot}$	$M_{\rm MS,f}$ ${\rm M}_{\odot}$	$M_{\rm wind}$ ${\rm M}_{\odot}$	M_7 ${\rm M}_{\odot}$	$\dot{M}_{\rm max}$ 10^{-7} ${\rm M}_{\odot}$ yr^{-1}	$L_{\rm X}$ 10^{38}erg s^{-1}	$X_{\rm c}$	$\tau_{\rm SN}$ 10^9 yr
(1)	(2)	(3)	(4)	(5)	(6)	(7)	(8)	(9)	(10)	(11)	(12)	(13)
0	2.4	1.0	1.69	1.49	1.05	-	0.03	0.04	11.0	1.63	0.08	-
1	2.3	1.0	0.51	0.27	1.94	1.58	0.28	0.80	7.47	1.57	0.69	0.01
2	2.3	1.0	1.74	0.90	1.93	1.47	0.39	0.81	8.68	1.77	0.07	0.79
3	2.1	1.0	1.65	1.11	1.85	1.66	0.00	0.72	3.90	1.85	0.08	1.06
4	2.0	1.0	0.69	0.49	1.80	1.56	0.00	0.63	3.75	1.66	0.46	0.77
5	2.0	1.0	1.07	0.76	1.77	1.56	0.00	0.63	3.49	1.54	0.24	1.08
6	2.0	1.0	1.29	0.91	1.75	1.56	0.00	0.60	3.03	1.34	0.17	1.17
7	2.0	1.0	1.63	1.16	1.69	1.55	0.00	0.52	2.35	1.04	0.07	1.26
8	2.0	1.0	1.73	1.22	1.70	1.55	0.00	0.52	2.27	1.00	0.03	1.30
9	1.8	1.0	0.54	0.42	1.54	1.35	0.00	0.25	1.45	0.64	0.60	0.70
10	1.8	1.0	0.95	0.74	1.53	1.35	0.00	0.28	1.43	0.63	0.28	1.50
11	1.8	1.0	1.14	0.88	1.48	1.35	0.00	0.15	1.10	0.48	0.20	1.85
12	1.8	1.0	1.22	0.94	1.46	1.35	0.00	0.00	0.97	0.43	0.17	1.89
13	1.8	1.0	1.25	0.97	1.45	1.35	0.00	0.00	0.92	0.40	0.15	1.92
14	1.8	1.0	1.33	1.02	1.44	-	0.00	0.00	0.83	0.37	0.11	1.96
22	1.74	1.0	0.57	0.47	1.48	1.29	0.00	0.16	1.16	0.51	0.53	1.21
23	1.74	1.0	0.63	0.52	1.48	1.29	0.00	0.18	1.23	0.54	0.46	1.70
24	1.74	1.0	0.96	0.77	1.44	-	0.00	0.00	0.94	0.42	0.27	2.01
25	2.1	0.8	0.59	0.28	1.00	-	0.28	0.12	10.5	1.05	0.52	-
26	2.1	0.8	0.94	0.42	0.98	-	0.32	0.12	10.3	1.05	0.30	-
29	2.1	0.8	1.19	0.43	1.44	0.74	0.72	0.55	10.9	1.05	0.19	0.96
30	2.1	0.8	1.23	0.44	1.45	0.75	0.71	0.54	10.6	1.05	0.17	0.98
31	2.1	0.8	1.53	0.58	1.49	0.79	0.66	0.58	9.80	1.05	0.09	1.05
32	2.0	0.8	0.60	0.28	1.56	1.05	0.31	0.61	4.49	1.05	0.51	0.66
33	2.0	0.8	0.78	0.35	1.54	1.02	0.35	0.61	4.72	1.05	0.37	0.90
34	2.0	0.8	1.55	0.76	1.60	1.12	0.24	0.63	4.45	1.05	0.08	1.25
35	2.0	0.8	1.79	0.75	1.60	0.66	0.69	0.63	9.08	1.05	0.01	1.31
36	1.9	0.8	0.60	0.33	1.44	1.17	0.09	0.61	3.16	1.05	0.56	0.50
37	1.9	0.8	1.66	0.87	1.44	0.93	0.33	0.64	5.05	1.05	0.01	1.61
38	1.8	0.8	0.58	0.36	1.50	1.15	0.00	0.50	2.08	0.92	0.53	1.16
39	1.8	0.8	1.36	0.83	1.46	1.15	0.00	0.45	1.85	0.82	0.08	2.00
40	1.7	0.8	0.66	0.43	1.38	-	0.00	0.33	1.40	0.62	0.44	-
41	1.7	0.8	0.76	0.50	1.38	-	0.00	0.34	1.41	0.62	0.37	-
42	1.7	0.8	0.81	0.53	1.37	-	0.00	0.32	1.38	0.61	0.34	-
43	1.7	0.8	1.01	0.66	1.35	-	0.00	0.24	1.21	0.53	0.22	-
44	1.7	0.8	1.33	0.87	1.62	1.06	0.00	0.33	1.38	0.61	0.02	2.75
45	1.7	0.8	1.50	0.98	1.69	1.06	0.00	0.51	1.99	0.88	0.00	2.76
46	1.6	0.8	0.70	0.47	1.25	-	0.00	0.00	0.79	0.35	0.42	-
47	1.6	0.8	1.11	0.75	1.24	-	0.00	0.00	0.83	0.37	0.09	-
48	1.6	0.8	1.27	0.89	1.51	0.96	0.00	0.37	1.53	0.67	0.00	3.61
49	2.0	0.7	0.47	0.25	0.81	-	0.18	0.10	8.42	1.20	0.64	-
50	2.0	0.7	1.49	0.71	0.84	-	0.22	0.13	8.63	1.21	0.07	-
51	1.9	0.7	0.48	0.25	0.87	-	0.26	0.16	8.73	1.28	0.53	-
52	1.9	0.7	1.47	0.55	1.31	-	0.57	0.48	6.74	0.68	0.07	-
53	1.8	0.7	1.37	0.63	1.37	-	0.27	0.51	3.46	0.68	0.06	-

Table 3. List of key properties of computed systems with $Z = 0.001$ (cf. Table 2).

Nr.	$M_{\rm MS,i}$ $\rm M_\odot$	$M_{\rm WD,i}$ $\rm M_\odot$	$P_{\rm i}$ d	$P_{\rm min}$ d	$M_{\rm CO}$ $\rm M_\odot$	$M_{\rm MS,f}$ $\rm M_\odot$	$M_{\rm wind}$ $\rm M_\odot$	M_7 $\rm M_\odot$	$\dot{M}_{\rm max}$ 10^{-7} $\rm M_\odot$ yr^{-1}	$L_{\rm X}$ 10^{38}erg s^{-1}	$X_{\rm c}$	$\tau_{\rm SN}$ 10^9 yr
(1)	(2)	(3)	(4)	(5)	(6)	(7)	(8)	(9)	(10)	(11)	(12)	(13)
54	1.9	1.0	0.31	0.22	1.77	1.25	0.21	0.68	8.69	1.64	0.61	0.25
55	1.9	1.0	0.46	0.32	1.73	1.12	0.34	0.43	11.4	1.70	0.32	0.54
56	1.9	1.0	0.53	0.45	1.09	-	0.06	0.08	11.4	1.68	0.24	-
57	1.9	1.0	0.61	0.52	1.08	-	0.05	0.07	11.3	1.66	0.17	-
58	1.9	1.0	0.74	0.65	1.07	-	0.04	0.06	11.2	1.66	0.06	-
59	1.9	1.0	0.79	0.70	1.06	-	0.04	0.06	11.1	1.65	0.05	-
60	1.8	1.0	0.29	0.22	1.77	1.31	0.04	0.43	5.74	1.69	0.67	0.18
61	1.8	1.0	0.70	0.52	1.77	1.07	0.29	0.43	10.3	1.80	0.07	0.79
62	1.7	1.0	0.29	0.23	1.68	1.25	0.00	0.42	4.10	1.70	0.68	0.20
63	1.7	1.0	0.66	0.53	1.75	1.13	0.13	0.43	7.27	1.80	0.07	0.92
64	1.6	1.0	0.29	0.24	1.56	1.15	0.00	0.42	2.85	1.69	0.69	0.20
65	1.6	1.0	0.64	0.54	1.70	1.13	0.03	0.43	5.04	1.80	0.08	1.10
66	1.5	1.0	0.28	0.25	1.42	-	0.00	0.24	1.68	0.75	0.74	-
67	1.5	1.0	0.61	0.54	1.59	1.06	0.00	0.42	3.36	1.48	0.08	1.32
68	1.4	1.0	0.29	0.26	1.30	-	0.00	0.05	1.47	0.65	0.74	-
69	1.4	1.0	0.43	0.40	1.42	-	0.00	0.27	1.73	0.76	0.27	-
70	1.4	1.0	0.58	0.53	1.45	0.96	0.00	0.32	2.09	0.92	0.09	1.60
71	1.8	0.8	0.24	0.17	0.92	-	0.18	0.12	9.73	1.06	0.67	-
72	1.8	0.8	0.68	0.61	0.83	-	0.03	0.03	8.70	1.05	0.07	-
73	1.7	0.8	0.66	0.55	0.85	-	0.05	0.05	8.96	1.05	0.06	-
74	1.6	0.8	0.29	0.19	1.44	-	0.11	0.53	4.24	1.05	0.67	0.26
75	1.6	0.8	0.62	0.40	1.39	-	0.33	0.50	6.58	1.05	0.07	-
76	1.5	0.8	0.28	0.21	1.37	-	0.00	0.44	2.65	1.05	0.70	-
77	1.5	0.8	0.60	0.43	1.40	-	0.14	0.50	4.42	1.05	0.07	-
78	1.4	0.8	0.29	0.23	1.22	-	0.00	0.22	1.58	0.70	0.73	-

3. Mass transfer and white dwarf evolution

3.1. Mass transfer rates

In this Section, we deal with the mass transfer rates $\dot{M}$, and we emphasize that the mass accumulation rate of the white dwarf $\dot{M}_{\rm WD}$ may be smaller than the mass transfer rate if the latter is above or below the threshold values defined in Sect. 2.1. We want investigate the dependence of the mass transfer rate, and of its time dependence, on the various initial parameters of our binary systems. Although Eq. 12 gives the order of magnitude of the mass transfer rate during the thermally unstable phase, we will see that it fails to reproduce all the physical dependences correctly.

First consider the dependence of the mass transfer rate on the initial mass of the main sequence component $M_{\rm MS,i}$. Figures 7 and 8 show the mass transfer rate as function of time for systems with white dwarf initial masses of $M_{\rm WD,i} = 1\,\rm M_\odot$ and various initial main sequence masses, for $Z = 0.02$ and $Z = 0.001$, respectively. For both metallicities, there is a clear trend to larger maximum mass transfer rates for more massive main sequence stars caused by the shorter thermal time scale of more massive main sequence stars. Eq. 12, with $\tau_{\rm KH} := GM^2/(2RL)$, does reproduce the maximum mass transfer rates within 30% for all sequences shown in Fig. 8. However, it overestimates those of the sequences shown in Fig. 7 by factors 3...8, larger values corresponding to smaller initial main sequence star masses.

In all our models, there is a the time delay from the onset of the mass transfer (defined as $t = 0$ in Figs. 7 and 8) to the time when the mass transfer rate has grown sufficiently to allow the white dwarf mass to grow. This delay is of the order of the thermal time scale of the main sequence star, i.e. it is longer for smaller masses. We emphasize that our method to compute the mass transfer rate (Ritter 1988, see also Braun 1997) allows its reliable computation also for the beginning and the end of the mass transfer evolution. Assuming a nova outburst would occur after the accumulation of $\sim 10^{-5}\,\rm M_\odot$ (cf. Prialnik & Kovetz 1995) and mass accretion rates of the order of $10^{-8}\,\rm M_\odot\ yr^{-1}$ — i.e. nova recurrence times of about 10^3 yr — implies of the order of thousand nova outbursts in our typical supernova Ia progenitors before the white dwarf mass can start growing.

Fig. 9 shows the mass transfer rate as a function of time for three systems with the same initial main sequence star mass but with different initial white dwarf masses. The time delay from the onset of the mass transfer until the mass transfer rate exceeds $\sim 10^{-8}\,\rm M_\odot\ yr^{-1}$ and the white dwarf mass can start growing is very similar for all three systems. The delay is determined by the thermal time scale of the main sequence star.

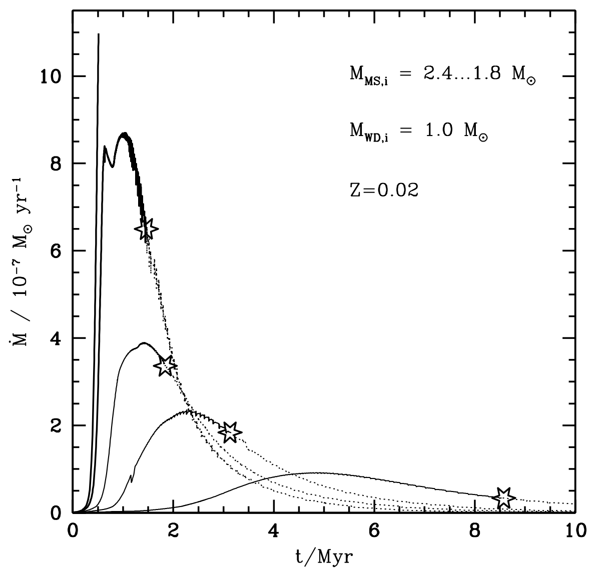

Fig. 7. Evolution of the mass transfer rate as function of time for systems No. 0, 2, 3, 7 and 13, which have a metallicity of Z=0.02 and white dwarf companions with initially $1\,M_\odot$ (see also Fig. 8). System No.0 (leftmost line) is stopped when the mass transfer rate exceeds the allowed upper limit for the wind mass loss rate (cf. Sect. 2.1). For the other four curves, higher peak mass transfer rates correspond to larger initial main sequence star masses ($2.3\,M_\odot$, $2.1\,M_\odot$, $2.0\,M_\odot$, and $1.8\,M_\odot$). The time $t = 0$ is defined by the onset of mass transfer. The star symbol indicates the time when the white dwarf has reached $1.4\,M_\odot$. Beyond that point, the graphs are continued as dotted lines.

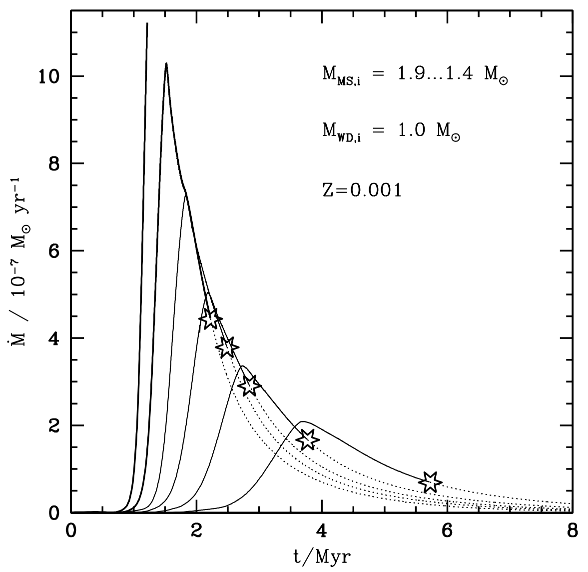

Fig. 8. Evolution of the mass transfer rate as function of time for low metallicity systems No. 58, 61, 63, 65, 67 and 70. The initial white dwarf mass is $1\,M_\odot$ for all six cases. Higher peak mass transfer rates correspond to larger initial main sequence star masses, from $1.9\,M_\odot$ to $1.4\,M_\odot$ in steps of $0.1\,M_\odot$. System No. 58 (leftmost line) is stopped when the mass transfer rate exceeds the allowed upper limit for the wind mass loss rate (cf. Sect. 2.1). Note that the scale of the vertical axis is identical to that in Fig. 7, but the represented initial masses of the main sequence components is lower.

Most striking in Fig. 9 is the feature that much larger mass transfer rates are achieved for smaller white dwarf masses. Although this trend is also expected from Eq. 12, the order of magnitude of the effect seen in Fig. 9 is much larger than what Eq. 12 predicts. We find that, although initially less massive white dwarfs need to accrete more mass to reach the Chandrasekhar mass, the best supernova Ia candidate system of those displayed in Fig. 9 may actually be the one with the *smallest* initial white dwarf mass. This is so since the same donor star transfers much more mass for smaller initial white dwarf masses, and that even at higher mass transfer rates.

For otherwise fixed system parameters, more mass is transfered for smaller initial white dwarf masses since the minimum orbital separation — coincides with the time when $M_{\rm MS} = M_{\rm WD}$ in the conservative case — is obtained only after more mass is transferred. Higher mass transfer rates are achieved since smaller minimum orbital separations are obtained for smaller values of $M_{\rm WD,i}$. For conservative evolution of a given binary system, the orbital separation d can be expressed as

$$d = J^2 \frac{M_{\rm MS} + M_{\rm WD}}{G M_{\rm MS}^2 M_{\rm WD}^2}, \tag{14}$$

where

$$J = \frac{2\pi d^2}{P} \frac{M_{\rm MS} M_{\rm WD}}{M_{\rm MS} + M_{\rm WD}} \tag{15}$$

is the constant orbital angular momentum. Therefore, a given initial separation $d_{\rm i}$ relates to the minimum orbital separation $d_{\rm min}$ as

$$\frac{d_{\rm min}}{d_{\rm i}} = \left(4 \frac{M_{\rm MS,i} M_{\rm WD,i}}{(M_{\rm MS,i} + M_{\rm WD,i})^2} \right)^2, \tag{16}$$

and as for fixed system mass the period and separations are related as $P^2 \propto d^3$ it is

$$\frac{P_{\rm min}}{P_{\rm i}} = \left(4 \frac{M_{\rm MS,i} M_{\rm WD,i}}{(M_{\rm MS,i} + M_{\rm WD,i})^2} \right)^3. \tag{17}$$

I.e., let us consider two main sequence stars of the same mass, starting to transfer mass onto their white dwarf companions at the same orbital separation $d_{\rm i}$. The minimum separation will be smaller for the binary with the smaller initial white dwarf mass, say System A. Since the radius of main sequence stars in the considered mass range decrease for increasing mass loss rates, the mass loss rate of the main sequence star in System A — i.e., its mass transfer rate — needs to be larger in order to fit the main sequence star into a smaller volume.

The fact that the white dwarf in System No. 53, which has an initial mass of $0.7\,M_\odot$, does not reach $1.4\,M_\odot$ but

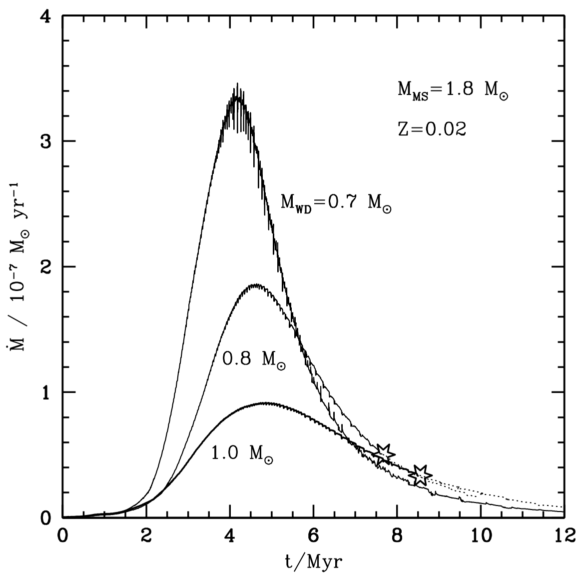

Fig. 9. Evolution of the mass transfer rate as function of time for systems No. 13, 39 and 53, i.e. systems with a metallicity of $Z = 0.02$ and with initial main sequence star masses of $1.8\,M_\odot$, but with three different initial white dwarf masses, as indicated. (Cf. also caption to Fig. 7.)

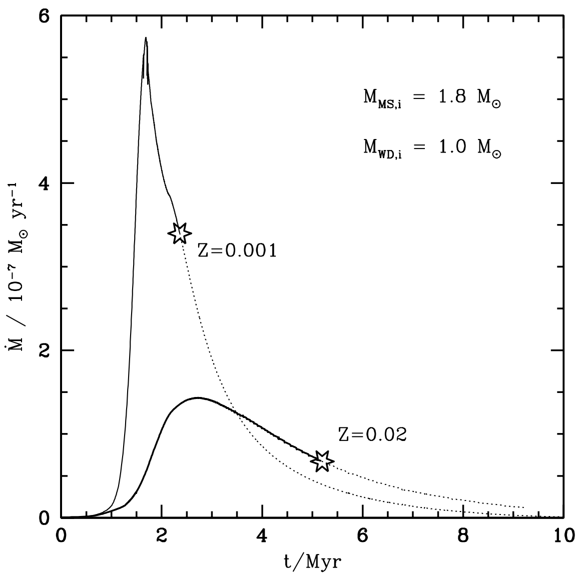

Fig. 10. Evolution of the mass transfer rate as function of time for systems No. 9 and 60, which have identical initial main sequence star and white dwarf masses, but different metallicities, as indicated. (Cf. also caption to Fig. 7.)

only $1.37\,M_\odot$ is due to the fact that during the peak of the mass transfer the rate slightly exceeds the Eddington accretion rate $\dot{M}_{\rm Edd}$ (which is smaller for smaller white dwarf masses; cf. Sect. 2.1), and this system loses $0.27\,M_\odot$ to a wind. The other two systems shown in Fig. 9, No. 13 ($M_{\rm WD,i} = 1\,M_\odot$) and No. 39 ($M_{\rm WD,i} = 0.8\,M_\odot$), which avoid winds, can grow the CO-white dwarf to $1.45\,M_\odot$ and $1.46\,M_\odot$, respectively. In fact, the system with the largest initial white dwarf mass, System No. 13, is least likely to produce a Type Ia supernova, since in this system all mass is transferred at rates below 10^{-7} $M_\odot$ yr^{-1}. I.e., $M_7 = 0$ in this case, while $M_7 = 0.45\,M_\odot$ for System No. 39, and $M_7 = 0.51\,M_\odot$ for System No. 53 (cf. Tab. 2).

I.e., the effect that systems with smaller initial white dwarf masses are better Type Ia supernova progenitor candidates is only limited by the smaller upper limits to the white dwarf mass accumulation rate for smaller white dwarf masses.

The dependence of the mass transfer rate on the metallicity of the main sequence star is elucidated in Fig. 10. It shows two systems with identical initial main sequence star and initial white dwarf masses but with different metallicities. Wind mass loss is negligible in both cases. The difference in the maximum mass transfer rate of Systems No. 9 and No. 60 — which both start with a main sequence star of $1.8\,M_\odot$ and a white dwarf of $1\,M_\odot$ — is a factor of four. Both systems have initial periods close to the shortest possible initial period. This large difference is *not* due to different stellar Kelvin-Helmholtz time scales $\tau_{\rm KH}$. Although the low metallicity stars are more luminous, they are also more compact both effects on $\tau_{\rm KH}$ almost cancel out (cf. also Table 1). At the onset of mass transfer, it is $\tau_{\rm KH} = 2.6$ Myr for the main sequence star in System No. 9, while the corresponding value for System No. 60 is $\tau_{\rm KH} = 2.4$ Myr. This is also reflected in the similarity of the turn-on times for the mass transfer (cf. Fig. 10).

Low metallicity systems have larger mass transfer rates compared to systems with solar abundances (Figs. 7 & 8). While the range of mass transfer rates covered in both figures is the same, Fig. 7 ($Z = 0.02$) shows systems with initial main sequence masses in the range 2.4...1.8 $M_\odot$, while those in Fig. 8 ($Z = 0.001$) are in the range 1.9...1.4 $M_\odot$. Based on our detailed models, Eq. 12 is valid for low metallicity within a factor of two. For solar metallicities, the mass transfer rates are systematically lower by a factor of 5. I.e., on average the low metallicity systems have, for the same initial stellar masses, five times higher mass transfer rates than the systems at $Z = 0.02$.

We want to point out that, for the Case A systems considered in this work, the maximum mass transfer rate can vary by up to a factor of 2 as function of the initial period (cf. Tables 2 and 3). One would expect larger mass transfer rates for initially wider systems, since in this case the main sequence star is more extended and more luminous at the onset of the mass transfer, and thus has a shorter Kelvin-Helmholtz time scales (cf. Table 1). This expectation, which is also reflected in Eq. 12, is fulfilled rather well for most of our low metallicity systems (cf. Table 3). However, at $Z = 0.02$ we find mostly decreasing maximum mass transfer rates for increasing initial periods and otherwise fixed initial system parameters (cf. Table 2). This means that Eq. 12 can not be used to predict trends of the mass transfer rate as function of the initial period or the system metallicity, and shows the limitations of simplifying approaches to the study of accreting white dwarfs in binary systems.

3.2. Evolution of the white dwarf mass

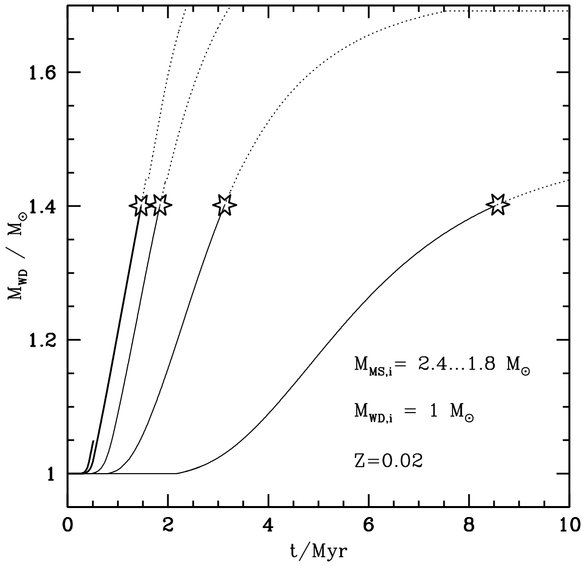

Fig. 11. Evolution of the white dwarf mass as function of time for systems No. 0, 2, 3, 7, and 13 (cf. Fig. 7.)

The dependence of the mass transfer rate on various parameters discussed in Section 3.3 has important implications for the evolution of the white dwarfs. Figs. 11 and 12 illustrate the time evolution of the white dwarf masses for the same systems for which the evolution of the mass transfer rate $\dot{M}$ has been displayed in Figs. 7 and 8. We recall that $|\dot{M}| \neq |\dot{M}_{\rm WD}|$ due to the restrictions on the mass accretion rate outlined in Section 2. I.e., the white dwarf mass can start to grow only 0.5...3 Myr after the onset of the mass transfer, due to the occurrence of nova outbursts (cf. also Section 3.3).

To demonstrate the effect of the upper and lower critical accretion rates for the achievable white dwarf masses, we have plotted in Fig. 13 the maximum possible CO-mass in the white dwarf — ignoring the possible occurrence of a supernova event at $M_{\rm WD} \simeq 1.4\,{\rm M}_\odot$ — as function of the initial main sequence mass for low metallicity systems with an initial white dwarf mass of $1\,{\rm M}_\odot$. The sharp drop of the curve at $M_{\rm MS,i} = 1.9\,{\rm M}_\odot$ is due to the fact that the mass accretion rate exceeds three times the Eddington accretion rate of the white dwarf shortly after the onset of the mass transfer in the system with $M_{\rm MS,i} = 1.9\,{\rm M}_\odot$, which

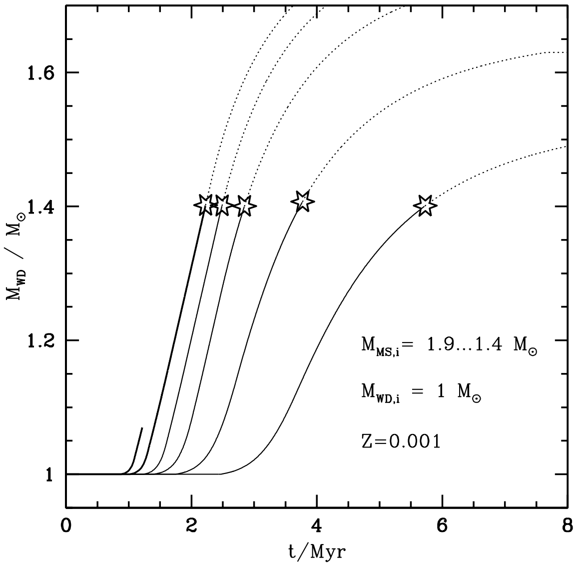

Fig. 12. Evolution of the white dwarf mass as function of time for systems No. 58, 61, 63, 65, 67 and 70 (cf. Fig. 8.)

we use as criterion to stop the calculations (cf. Section 2), assuming that the white dwarf would form an extended hydrogen-rich envelope and the two stars in the system would merge.

Fig. 13 also shows the sum of $M_{\rm CO}$ and the total amount of mass lost from the system due to a white dwarf wind (see also Tables 2 and 3). It indicates that winds, and thus the upper critical accretion rate, are unimportant for initial main sequence masses $M_{\rm MS,i} \lesssim 1.6\,{\rm M}_\odot$, at $Z = 0.001$. As the wind efficiency is quite uncertain (cf. Section 2, and Kobayashi et al. 1998), the maximum main sequence mass in Type Ia supernova progenitor systems of Case A is somewhat uncertain. However, as the maximum mass transfer rate rises very sharply with increasing initial main sequence mass (Figs. 7 and 8), the maximum main sequence mass is not very sensitive to the assumptions on the wind mass loss rate. E.g., Li & van den Heuvel (1997), following Hachisu et al. (1996), allowed wind mass loss rates of up to $10^{-4}\ {\rm M}_\odot\ {\rm yr}^{-1}$, i.e. roughly 100 times more than in our calculations. This shifts the maximum main sequence mass from $2.3\,{\rm M}_\odot$ in our case to $2.6\,{\rm M}_\odot$ in their case, for Case A systems with an initial white dwarf mass of $1\,{\rm M}_\odot$ and a metallicity of 2%.

The lower curve in Fig. 13 shows $M_{\rm WD,i} + M_7$, i.e. the maximum achievable CO mass assuming that mass accumulation on the white dwarf is only possible for $\dot{M} > 10^{-7}\ {\rm M}_\odot\ {\rm yr}^{-1}$ (cf. Eq. 13). It shows that under these assumptions the white dwarfs in the low metallicity systems with initial main sequence masses in the range $1.5...1.8\,{\rm M}_\odot$ would still be able to grow to $1.4\,{\rm M}_\odot$, although not to significantly larger values.

Figs. 14 and 15 show the complete picture of the outcome of our study for the achievable white dwarf mass as

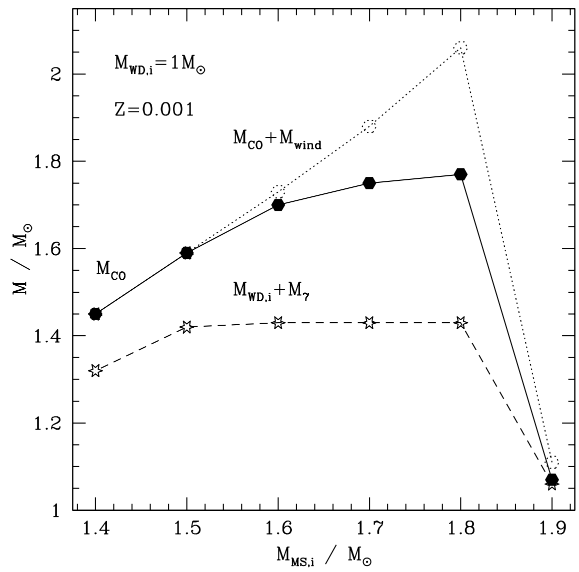

Fig. 13. Maximum achievable CO-mass $M_{\rm CO}$ (see text; solid line and solid dots), $M_{\rm CO}$ plus the total mass lost to a wind (dotted line and dots), and initial white dwarf mass ($1\,{\rm M}_\odot$ for all systems shown here) plus M_7 (cf. Eq. 13) — i.e. the at least achieved CO-mass in the white dwarf — for the low metallicity systems No. 58, 61, 63, 65, 67 and 70 (cf. Figs. 7 and 12, and also Figs. 16 and 17).

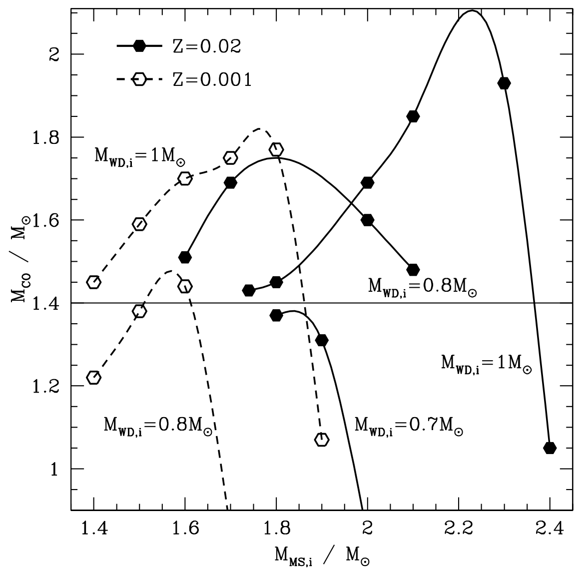

Fig. 14. Maximum achievable CO-core masses as function of the initial mass of the main sequence star, for various initial white dwarf masses and for the two metallicities considered here, as indicated (cf. also Figs. 13 and 17).

function of the system parameters. While Fig. 14 gives the optimistic view, i.e. applying the lower critical accretion rates defined in Section 2, Fig. 15 gives the pessimistic view by showing graphs for $M_{\rm WD,i} + M_7$ rather than for $M_{\rm CO}$. When considering Figs. 14 and 15, it is important to keep in mind that the variation of the initial period of the considered systems would convert each line in these figures into a band with an average width of the order of $0.1\,{\rm M}_\odot$ (cf. Tables 2 and 3). These figures allow the following conclusions.

1. The initial main sequence masses from which Type Ia supernovae at low metallicity can be drawn ($\sim 1.45\,{\rm M}_\odot ... 1.85\,{\rm M}_\odot$) are much smaller than at $Z = 0.02$ ($\sim 1.7\,{\rm M}_\odot ... 2.35\,{\rm M}_\odot$).
2. The initial masses of the white dwarfs required for a Type Ia supernova are — on average — about $0.2\,{\rm M}_\odot$ larger at $Z = 0.001$ compared to the high metallicity systems. I.e., note that in Figs. 14 and 15 the curves for $M_{\rm WD,i} = 1\,{\rm M}_\odot$ at $Z = 0.001$ are similar to those for $M_{\rm WD,i} = 0.8\,{\rm M}_\odot$ at $Z = 0.02$, only shifted to lower initial main sequence star masses.
3. Since smaller initial mass ratios $M_{\rm WD,i}/M_{\rm MS,i}$ lead to larger mass transfer rates, more mass is transfered in systems with smaller initial white dwarf masses than for lower initial white dwarf masses. This effect may give systems with small initial white dwarf masses — i.e. perhaps as low as $M_{\rm WD,i} = 0.7\,{\rm M}_\odot$ at $Z = 0.02$ and $0.7\,{\rm M}_\odot$at $Z = 0.001$ — the possibility to produce a Type Ia supernova.

4. Evolution of further system parameters

4.1. White dwarf spin

In Sect. 2.2, we showed that, within simple approximations, the spin of the accreting white dwarfs at any given time depends only on the amount of matter accreted up to that time. From Eq. 9 follows that the largest spin at the time of the supernova explosion is expected in those systems that start out with the least massive white dwarfs. For initial white dwarf masses of $1.2\,{\rm M}_\odot$, $1.0\,{\rm M}_\odot$, $0.8\,{\rm M}_\odot$, and $0.7\,{\rm M}_\odot$, the assumption of homogeneous white dwarfs (i.e., $k^2 = \frac{2}{5}$) leads to ratios of rotational to critical rotational velocity Ω of 0.35, 0.67, 0.98, and 1.13, respectively. A more realistic value of $k = 0.4$ (Ritter 1985) results even in $\Omega = 0.85$, 1.68, 2.45, and 2.83. While these numbers should not be taken literally — in particular, values of $\Omega > 1$ are of course not plausible — they elucidate the possibility that many of the exploding white dwarfs in Type Ia supernovae may be rotating at a speed close to break-up. According to Figs. 14 and 15 it is not excluded that white dwarfs with initial masses of $\sim 0.7\,{\rm M}_\odot$ may contribute to the Type Ia supernovae, even at low metallicity.

This point of view is at least partly supported by observational evidence. While isolated white dwarfs appear to rotate very slowly ($v_{\rm rot} \lesssim 50\,{\rm km\,s}^{-1}$; Heber et al. 1997, Koester et al. 1998) — which is also expected from recent

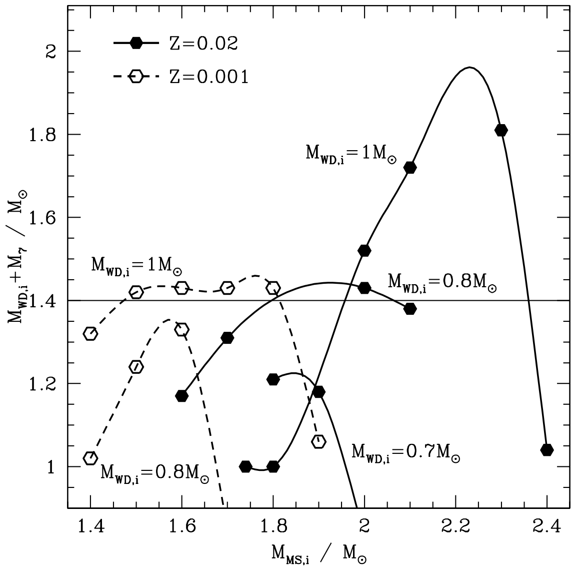

Fig. 15. CO-core masses achieved if only mass accreted with rates above 10^{-7} $M_\odot$ yr^{-1} are considered, as function of the initial mass of the main sequence star, for various initial white dwarf masses and for the two metallicities considered here, as indicated (cf. also Figs. 13 and 16).

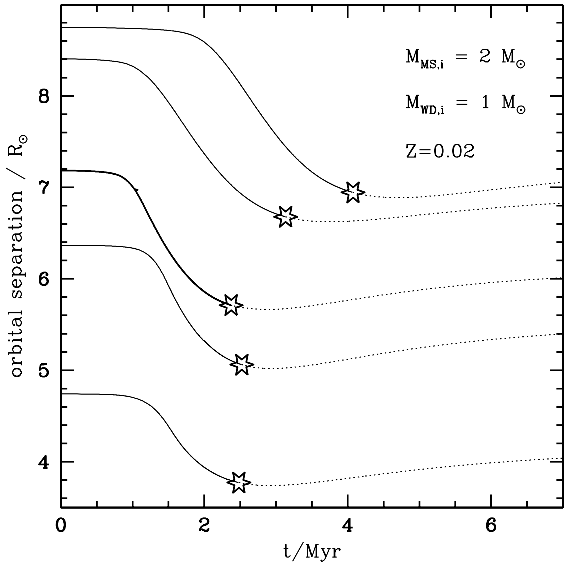

Fig. 16. Evolution of the orbital separation as function of time for systems No. 4, 5, 6, 7, and 8. The time $t = 0$ is defined by the onset of mass transfer. A star symbol indicates the time when the white dwarf has reached $1.4\,M_\odot$. Beyond that point, the graphs are continued as dotted lines.

single star models with rotation (Langer et al. 1999) — those in CVs can be much larger, i.e. up to $1200\,\mathrm{km\,s^{-1}}$ (Sion 1999). As the white dwarfs in CVs are accreting, this shows that accreting white dwarfs are in fact spun-up. The fact that the white dwarfs in CVs are not spinning as rapidly as expected from Eq. 9 is interpreted by Livio & Pringle (1998) as being due to angular momentum loss in nova explosions which must occur in typical CV systems.

From our simple approach, we expect that by the time the white dwarf mass gets close to the Chandrasekhar limit, it may rotate with a significant fraction of the break-up velocity. First polarization studies of Ia supernovae seem to indicate that the degree of polarization in the supernova spectra is very low (Wang et al. 1996), which makes a strongly deformed white dwarf as initial configuration for the explosion rather unlikely. A confirmation of these results on a solid statistical basis would imply that either typical initial white dwarf masses are rather high, or that the white dwarfs can lose angular momentum during their accretion phase through mechanisms yet to be found.

4.2. Orbital evolution

In all systems the mass transfer rate remains initially on a low level for about one Kelvin-Helmholtz time scale of the main sequence star. Nova outbursts are to be expected for the first 0.5...2 Myr of the mass transfer evolution. This is simulated as a continuous process in our calculations, where all transferred mass leaves the system immediately, carrying the specific orbital angular momentum of the white dwarf. Both, mass transfer and nova winds at this stage ($M_{\rm MS} > M_{\rm WD}$) lead to a decrease of the orbital separation. The effective shrinkage of the orbit is, however, small since the amounts of mass involved in the mass transfer and winds during this phase are small (cf. Sect. 3). We have not included the possibility of frictional angular momentum loss during nova outbursts (e.g., Livio & Pringle 1998), as this could have been compensated by a slight increase of our initial periods which are treated as a free parameter anyway.

Once the mass transfer rate exceeds the critical rates $\dot{M}_{\rm H}$ and $\dot{M}_{\rm He}$ (cf. Sect. 2), we assume the mass transfer to be conservative as long as $\dot{M} \leq \dot{M}_{\rm Edd}$ (Eq. 1). In that case, mass and angular momentum conservation lead to a shrinkage of the orbit as long as $M_{\rm MS} > M_{\rm WD}$, and to a widening thereafter. Fig. 16 shows the evolution of the orbital separation with time for five systems with the same initial main sequence star and white dwarf mass but with different initial periods. As none of these systems develops a super-Eddington wind, the minimum orbital separations follow from Eq. 16 (neglecting the nova winds). As Eq. 17 can be expressed as

$$P_{\rm min} = P_{\rm i} \left(\frac{4q_i}{(q_i+1)^2} \right)^3 , \qquad (18)$$

using $q_i = M_{\rm WD,i}/M_{\rm MS,i}$, shorter minimum periods are achieved for shorter initial periods, and for smaller initial mass ratios $q_i < 1$.

Those systems which evolve a super-Eddington wind can evolve to considerably shorter periods than the conservative systems (Eq. 17). The main reason is that the condition $M_{\rm MS} > M_{\rm WD}$ remains fulfilled for a much longer time than in the conservative case. E.g., Systems No. 1 and No. 2, which lose about $0.28\,M_\odot$ and $0.39\,M_\odot$ to a wind, evolve to minimum periods of 6.5 h and 21.6 h, respectively (cf. Table 1), while their minimum periods in a conservative evolution would have been 7.5 h and 25.2 h.

4.3. Evolution of the main sequence star

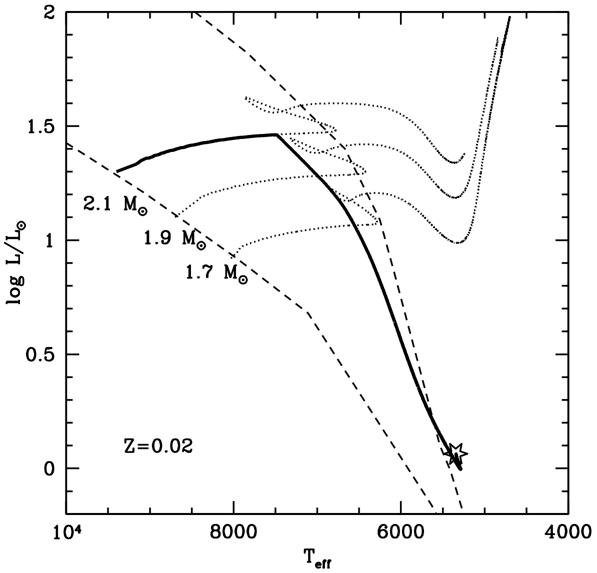

Fig. 17. Evolutionary track in the HR diagram of the main sequence component of a $2.1\,M_\odot$+$0.8\,M_\odot$ main sequence star + white dwarf binary with a metallicity of 2% and an initial period of 1.23 d (System No. 30), from zero age until the supernova explosion of the white dwarf (thick solid line). Dotted lines correspond to evolutionary tracks of single stars of 2.1, 1.9, and $1.7\,M_\odot$. The two dashed lines denote the zero age main sequence (left line) and the terminal age main sequence (corresponding to core hydrogen exhaustion). The star symbol denotes the time when the white dwarf reaches $1.4\,M_\odot$.

A discussion of the properties of the main sequence stars in the supernova Ia progenitor systems presented before may be interesting for two reasons. First, it might be observable during the accretion phase, where our systems might appear as supersoft X-ray sources. Second, the main sequence star may survive the explosion of the white dwarf and may then serve as an observable witness of the supernova progenitor evolution.

To elucidate the first point, we have plotted in Fig. 17 the evolutionary track of the main sequence component of System No. 30 in the HR diagram, in comparison to normal single stars tracks for comparable initial masses. It is evident that this star, once the Roche lobe overflow sets in, reduces its luminosity significantly, roughly by a factor of ~ 30. However, from Fig. 17 it is not clear which fraction of the luminosity decrease is due to the fact that the stellar mass of the main sequence star becomes smaller — from $2.1\,M_\odot$ to about $0.8\,M_\odot$ at the time when the white dwarf has reached $1.4\,M_\odot$ —, and which fraction is due to the deviation of the star from global thermal equilibrium during the rapid mass loss phase.

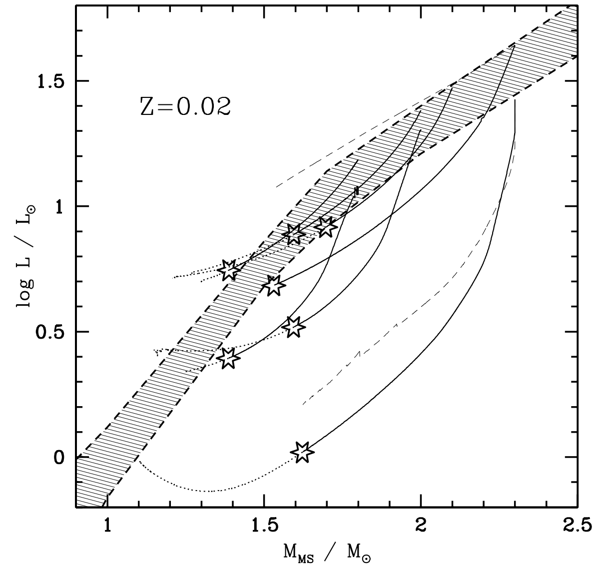

Fig. 18. Evolutionary tracks of the main sequence stars in the mass-luminosity diagram starting at the onset of mass transfer, for the $Z = Z_\odot$ Systems No. 1, 2, 3, 4, 7, 9, 13 (identifiable by the corresponding initial main sequence star masses, where the main sequence star of two systems with the same initial main sequence star mass has a larger initial luminosity for the system with the larger initial period). The tracks are shown as continuous lines up to the point when the white dwarf reaches $1.4\,M_\odot$, and are then continued as dotted lines (cf. Section 3). The shaded band is limited by the dot-dashed lines connecting the zero age and the terminal age main sequence positions of single stars in the mass range $0.8...3\,M_\odot$, taken from Schaller et al. (1992). The two dashed lines give the evolution of the nuclear luminosity $L_{\rm nuc} = \int_m \varepsilon_{\rm nuc} dm$ as function of the main sequence star mass from the onset to the mass transfer to the time when the white dwarf reaches $1.4\,M_\odot$, for Systems No. 1 (lower line) and No. 2 (upper line).

In order to understand which luminosities the main sequence components of our systems can achieve in general, and to what extent the reduction of the luminosity can be understood in terms of the mass reduction, we show in Figs. 18 and 19 the mass-luminosity evolution for a sample of our systems in comparison with the mass-luminosity relation for normal main sequence stars, for $Z = 0.02$ and $Z = 0.001$, respectively. These figures show that in most systems the main sequence components are significantly underluminous with respect to their mass.

The inspection of Figs. 18 and 19 reveals the following features. First, the systems with the shorter initial peri-

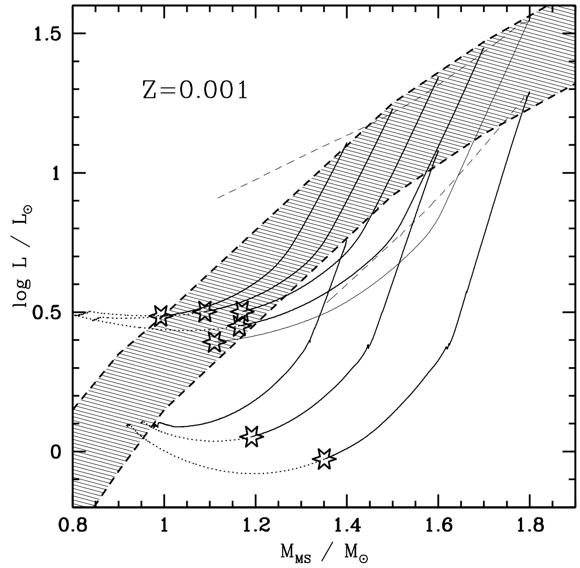

Fig. 19. Same as Fig. 18, but for our $Z = 0.001 Z_\odot$ Systems No. 60, 61, 63, 64, 65, 67, 68, and 70. The evolution of the nuclear luminosity is shown for Systems No. 60 (lower line) and No. 61(upper line).

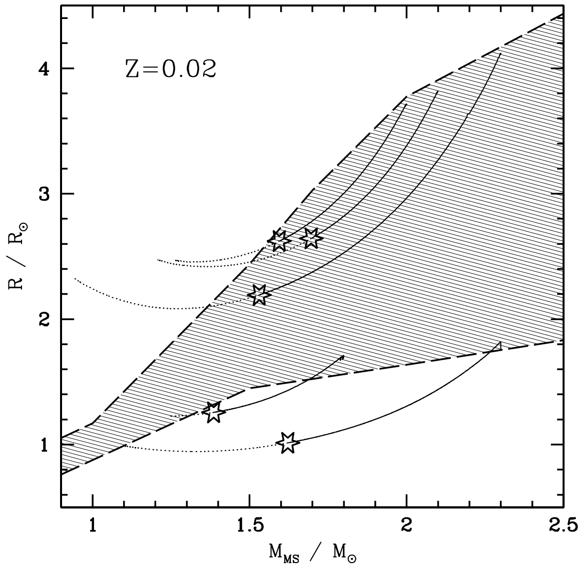

Fig. 20. Evolutionary tracks of the main sequence stars in the mass-radius diagram starting at the onset of mass transfer, for the $Z = Z_\odot$ Systems No. 1, 2, 3, 7, 9 (identifiable by the corresponding initial main sequence star masses, where the main sequence star of two systems with the same initial main sequence star mass has a larger initial radius for the system with the larger initial period). The tracks are shown as continuous lines up to the point when the white dwarf reaches 1.4 $M_\odot$, and are then continued as dotted lines (cf. Section 3). The shaded band is limited by the dot-dashed lines connecting the zero age and the terminal age main sequence positions of single stars in the mass range 0.8...3 $M_\odot$, taken from Schaller et al. (1992).

ods, which start out at the lower boundary of the main sequence band in these figures, evolve to the zero age main sequence position corresponding to their final mass once the mass transfer rates become small and thermal equilibrium is restored. In real binaries the white dwarf might explode before this happens, but the models shown in Figs. 18 and 19 are followed up to the end of the thermally unstable mass transfer phase, which corresponds to the endpoint of the dotted parts of the tracks. This result is easily understood, since when the mass transfer starts these stars are very unevolved, i.e. their internal hydrogen and helium distribution is basically homogeneous. Therefore, when these stars have lost a significant part of their initial mass, the spatial distribution of their main constituents (H and He) is still the same as in a zero age main sequence star. Since the stellar structure adjusts according to the chemical profiles, and once the mass transfer rate has dropped and the star can relax to thermal equilibrium, their properties can not be distinguished from those of normal main sequence stars of the same mass (except for trace elements; see below).

The deviation of these stars from the zero age main sequence mass-luminosity relation is due to the thermal imbalance. Due to the strong mass loss, the outer stellar layers expand which consumes energy and reduces the stellar luminosity as long as the strong mass loss prevails — strong meaning that the mass loss time scale is of the same order as the stellar Kelvin-Helmholtz time scale. This effect by itself can reduce the stellar luminosity by as much as a factor of 10 (Figs. 18 and 19), i.e., the star can appear ten times dimmer than expected from the mass-luminosity relation of single stars on the basis of its actual mass. The effect is stronger for larger mass loss rates. We emphasize that this reduction of the stellar luminosity due to the mass loss induced thermal imbalance comes actually in two components. One is that due to the strong mass loss, the outer stellar layers expand which consumes energy and reduces the stellar luminosity below the "nuclear luminosity", i.e. the amount of energy liberated by thermonuclear reactions in the stellar core. However, as main sequence stars adjust their nuclear luminosity to the radiative energy loss at the surface (Kippenhahn & Weigert 1990), also the nuclear luminosity of the mass losing main sequence stars is smaller than the nuclear luminosity of a non-mass losing main sequence star of the same mass and evolutionary stage (see Figs. 18 and 19).

For systems with a relatively large initial period, i.e. those where the mass transfer starts when the main sequence star is close to the terminal age main sequence (upper borderline of the main sequence band in Figs. 18 and 19), one phenomenon counterbalances the two dimming effects (i.e. mass reduction and thermal imbalance). The cores of these stars are, at the onset of the mass transfer, very helium-rich. Therefore, after the mass transfer they have a helium-rich core which is significantly more massive than a helium core in a single stars of the same stellar mass. This makes the stars overluminous compared to single stars, as can be seen from the dotted parts of the stellar tracks of the long-period systems shown in Figs. 18 and 19. Evidently, this effect — we call it the helium effect — is the larger the later the mass transfer starts during the core hydrogen burning evolution of the main sequence component, and the larger the total amount of mass lost.

In summary, we have three effects changing the luminosity of our main sequence component. First, as its mass is reduced, its luminosity is reduced according to the mass-luminosity relation of single stars (the mass effect). Second, the larger the mass loss or mass transfer rate the more is its luminosity reduced in addition, due to the thermal imbalance imposed by the mass loss (the mass loss effect). Third, the helium effect can lead to an increase of the luminosity for those stars which started out with (and therefore still have) relatively large periods. All together, we see from Figs. 18 and 19 that during the thermally unstable mass transfer phase no star can be found above the single star mass-luminosity band. On the other hand, a significant fraction of them is found below this band, at luminosities between 1 and $10\,L_{\odot}$.

Fig. 20 shows, for the case of the metal-rich stars, that not only the luminosities but also the radii of the mass transferring main sequence stars are significantly smaller than the radii of stars in thermal equilibrium with the same mass and evolutionary stage. Note that there is also a strong dependence of the main sequence star radii on metallicity (cf. Figs. 1 and 2 in Sect. 2.3). Both effects may be quite relevant for the derivation of component masses in supersoft X-ray binaries (cf. Sect. 5.1).

5. Observable consequences

5.1. Supersoft X-ray sources

White dwarfs which accrete hydrogen at such a rate that they can perform non-explosive hydrogen burning at their surface constitute the leading model for the persistent supersoft X-ray sources (SSSs, Kahabka & van den Heuvel 1997). Here, we want to compare our results to observations of SSSs. It is important to keep in mind that we restricted the parameter space of our models according to the possibility to obtain a Type Ia supernova. I.e., although all our models may be considered as models for SSSs, it is not excluded that the average SSSs have in fact quite different properties than our models. We therefore restrict ourselves to investigate three basic observable properties, i.e. the X-ray luminosity, the system period, and the luminosity of the donor star, and rather focus on what the largest and smallest of these values are rather than considering a typical average. For this purpose, we have compiled in Table 4 system properties at the time of the maximum X-ray luminosity — i.e., at the time of the maximum mass accumulation rate of the white dwarf, as we assume $L_X = \varepsilon \dot{M}_{\rm WD}$ (cf. Sect. 2.1).

The maximum X-ray luminosity which we can achieve in principle within our assumptions is that obtained by a Chandrasekhar-mass white dwarf accreting at its Eddington-rate (cf. Sect. 2.1), i.e. $2.07\,10^{38}\,{\rm erg\,s^{-1}}$. The largest value actually occurring in our models is $1.85\,10^{38}\,{\rm erg\,s^{-1}}$ (cf. Tab. 4). So far, none of the empirical bolometric fluxes derived from SSSs exceeds this value, although some are quite close to it (Kahabka & van den Heuvel 1997).

For comparing the periods of our models with those of SSSs, we focus on the short periods, since also post main sequence donor stars can produce SSSs which would occur in longer period systems (Li & van den Heuvel 1997, Hachisu et al. 1999, Wellstein et al. 1999b). At $Z = 0.02$, we find periods in the range 1.8...0.25 d (43...6 h), while at $Z = 0.001$ periods range from 19...5 h (cf. Tabs. 2 and 3). Observed periods in close binary SSSs (Kahabka & van den Heuvel 1997) are generally in good agreement with these figures.

Some authors in the literature express the necessity to explain the shortest periods found in SSSs with alternative scenarios. E.g., the SMC system 1E0035.4-7230 has a period of 4.1 h (Schmidtke et al. 1996), for which van Teeseling & King (1998) proposed a wind-driven evolution, with a very low mass main sequence star losing mass induced by the strong X-ray radiation of the white dwarf. We note that in particular our low-Z models show periods as low as 4 h (e.g., System No. 71 in Table 3). Furthermore, according to Eq. 18 *significantly* smaller periods are achievable for smaller but still plausible initial mass ratios. I.e., a system starting out with a $2.4\,M_{\odot}$ main sequence star and a $0.6\,M_{\odot}$ white dwarf could reduce is initial period by a factor 4. Thereby, even periods in the range 2...3 h could be obtained. Even though such systems might not lead to Type Ia supernovae, some of them may still allow for stationary hydrogen burning on the white dwarf surface for a limited amount of time.

Rappaport et al. (1994), in a population synthesis study of SSSs, considered all possible initial masses and periods. The shortest periods they find are of the order of 5 h. They consider only one metallicity (solar), for which the smallest period we found is ~ 6 h. In our low metallicity systems, we find a minimum of 4 h. Thus, also from to the results of Rappaport et al. we would expect then minimum periods as low as 3 h at low metallicity. Therefore, periods as short as that found in 1E0035.4-7230 may still be explained within the standard model of thermally unstable mass transfer studied in the present paper.

Finally, we want to discuss the brightness of the donor stars in our models, in relation to the fact that so far none of them could be observationally identified. In Sect. 4.2 we have seen that the main sequence stars in our models are, during the mass transfer phase, significantly underluminous for their actual mass. In Table 4, we show the

Table 4. Properties of selected systems at the time of the maximum X-ray luminosity. The columns have the following meanings. (1) system number (cf. Tables 2 and 3), (2) main sequence star initial mass, (3) white dwarf initial mass, (4) initial period, (5) mass transfer rate, (6) mass accumulation rate of white dwarf, (7) white dwarf luminosity (8) Eddington luminosity of white dwarf (9) effective temperature of white dwarf, (10) white dwarf mass, (11) main sequence star mass, (12) main sequence star luminosity, (13) effective temperature of main sequence star, (14) orbital period (15) orbital velocity of main sequence star, (16) orbital velocity of white dwarf.

#	$M_{\rm MS,i}$	$M_{\rm WD,i}$	$P_{\rm i}$	$\dot{M}$ 10^{-7}	$\dot{M}_{\rm WD}$ 10^{-7}	L_X 10^{38}	$L_{\rm Edd}$ 10^{38}	$T_{\rm WD}$ 10^3	$M_{\rm WD}$	$M_{\rm MS}$	$L_{\rm MS}$	$T_{\rm MS}$ 10^3	P	$v_{\rm MS}$	$v_{\rm WD}$
	$M_\odot$	$M_\odot$	d	$M_\odot$/yr	$M_\odot$/yr	erg/s	erg/s	K	$M_\odot$	$M_\odot$	$L_\odot$	K	d	km/s	km/s
(1)	(2)	(3)	(4)	(5)	(6)	(7)	(8)	(9)	(10)	(11)	(12)	(13)	(14)	(15)	(16)
1	2.3	1.0	0.51	7.47	3.87	1.57	1.57	818	1.06	1.91	2.00	6.26	0.32	160	288
3	2.1	1.0	1.65	3.90	3.90	1.85	1.85	877	1.25	1.83	10.7	6.17	1.23	117	172
4	2.0	1.0	0.69	3.75	3.75	1.66	1.66	837	1.12	1.87	7.03	7.02	0.59	137	229
9	1.8	1.0	0.54	1.45	1.45	0.64	1.64	648	1.11	1.67	5.01	7.09	0.47	154	231
29	2.1	0.8	1.19	2.39	2.39	1.05	1.51	734	1.02	1.43	1.90	5.73	1.14	114	160
34	2.0	0.8	1.55	2.38	2.38	1.05	1.57	739	1.06	1.60	5.56	5.96	1.37	106	160
36	1.9	0.8	0.60	2.40	2.38	1.05	1.30	744	0.88	1.82	6.35	7.10	0.54	118	245
38	1.8	0.8	0.58	2.08	2.08	0.92	1.30	756	0.88	1.57	5.37	7.01	0.50	130	232
40	1.7	0.8	0.66	1.40	1.40	0.62	1.41	636	0.95	1.54	3.98	6.58	0.50	139	225
49	2.0	0.7	0.47	8.05	2.67	1.20	1.20	731	0.81	1.71	1.26	6.07	0.25	148	312
51	1.9	0.7	0.48	8.60	2.87	1.28	1.28	751	0.87	1.46	0.86	5.73	0.25	167	280
54	1.9	1.0	0.31	6.92	3.70	1.64	1.64	833	1.11	1.64	1.80	6.90	0.23	196	290
60	1.8	1.0	0.29	5.21	3.81	1.69	1.69	843	1.14	1.60	2.17	7.27	0.24	200	280
62	1.7	1.0	0.29	4.07	3.86	1.70	1.70	845	1.15	1.54	2.58	7.54	0.25	127	170
64	1.6	1.0	0.29	2.85	2.85	1.25	1.69	783	1.14	1.46	2.65	7.62	0.25	204	261
67	1.5	1.0	0.61	3.36	3.36	1.48	1.70	817	1.15	1.35	5.62	7.25	0.54	164	192
70	1.4	1.0	0.58	2.09	2.09	0.92	1.67	724	1.13	1.26	5.04	7.19	0.53	167	186
71	1.8	0.8	0.24	9.73	2.38	1.06	1.36	725	0.92	1.50	0.65	5.97	0.18	194	314

properties of the main sequence stars at the time of the maximum X-ray luminosity, for selected cases. Comparing Systems No. 1 and No. 3, we see that the stellar luminosity is not well correlated with the mass of the main sequence star. Instead, it is inversely correlated with the mass transfer rate, i.e. the mass loss rate of the main sequence star. For systems which have no wind, i.e. for which $\dot{M} = \dot{M}_{\rm WD}$ and thus $L_X \propto \dot{M}$, this means that the brighter the system in X-rays, the dimmer is the main sequence star. I.e., the fact that in the supersoft X-ray sources the X-ray luminosity is large (otherwise we would not notice them) means that the mass transfer rate must also be large (cf. Section 4.3). We conclude that the reduction of the main sequence star luminosity due to the thermal imbalance must be a large effect in observed supersoft sources of the considered type. As it can reduce the bolometric luminosity of the main sequence star by more than one order of magnitude, it may be quite difficult to observe the main sequence component in supersoft X-ray binaries.

5.2. The stellar remnant

Once the white dwarf has exploded, the main sequence component is likely to survive, and although some small amounts of mass may be stripped off by the supernova ejecta and blast wave, (Wheeler et al. 1975, see also Fryxell & Arnett 1981, Taam and Fryxell 1984), most stellar properties of our main sequence components will remain more or less unchanged. One may hope to identify and observe the remaining main sequence component either in a young Galactic supernova remnant produced by a Type Ia supernova, or, if they stick out sufficiently, long after the supernova explosion in the field.

In the first case, the thermal imbalance imposed by the mass transfer (cf. Sect. 4.4) will still be completely preserved, since the thermal time scale of the star is of the order of 10^7 yr, while any gaseous supernova remnant would dissolve at least 100 times faster. The expected luminosities of the main sequence components in a supernova Ia remnant can thus be directly read off Figs. 18 and 19 from the star-symbols, which mark the expected time of the supernova explosion. They are found to be in the range $1...10\,L_\odot$. When inspecting the effective temperatures of the main sequence stars at the time of the supernova, we find them to be systematically 500...1000 K cooler than single main sequence stars of the same mass and evolutionary state (Fig. 17; see also column 14 in Tab. 4). As the main sequence band has a width of more than 1000 K, this implies that remnant stars will be located on the main sequence band or slightly to the right. At $Z = 0.02$, the effective temperatures of the remnant stars are larger than

Table 5. Ratios of surface abundance of the main sequence star to initial abundance, at the time of the supernova explosion. The abundaces of all isotopes of the light elements Li, Be, and B are zero for all models.

Nr.	$M_{\rm MS,i}$ $M_\odot$	$M_{\rm MS,f}$ $M_\odot$	ΔM $M_\odot$	$\Delta M_{\rm wind}$ $M_\odot$	^{3}He	^{4}He	^{12}C	^{13}C	^{14}N	^{15}N	^{16}O	^{17}O	^{18}O	^{23}Na
3	2.1	1.66	0.44	0.00	6.71	1.00	1.00	1.00	1.00	1.00	1.00	1.00	1.00	1.00
8	2.0	1.55	0.45	0.00	7.91	1.00	1.00	1.00	1.00	1.00	1.00	1.00	1.00	1.00
13	1.8	1.35	0.45	0.00	14.8	1.00	1.00	1.00	1.00	1.00	1.00	1.00	1.00	1.00
29	2.1	0.74	1.36	0.72	4.33	1.00	0.08	2.22	4.61	0.06	1.00	2.92	0.02	1.06
31	2.1	0.79	1.31	0.66	6.65	1.04	0.15	3.66	4.28	0.07	1.00	2.39	0.05	1.07
32	2.0	1.05	0.95	0.31	7.45	1.01	0.91	7.28	1.12	0.34	1.00	1.00	0.77	1.00
35	2.0	0.66	1.34	0.69	4.10	1.07	0.08	1.91	4.60	0.06	0.99	6.27	0.03	1.07
36	1.9	1.17	0.73	0.09	16.8	1.01	0.99	1.48	1.00	0.89	1.00	1.00	0.99	1.00
37	1.9	0.93	0.97	0.33	14.4	1.03	0.69	10.7	1.80	0.22	1.00	1.02	0.46	1.00
38	1.8	1.15	0.65	0.00	22.6	1.00	0.99	1.10	1.00	0.97	1.00	1.00	0.99	1.00
39	1.8	1.15	0.65	0.00	26.9	1.01	0.99	1.30	1.00	0.93	1.00	1.00	0.99	1.00
45	1.7	1.06	0.64	0.00	28.1	1.01	0.99	1.64	1.00	0.90	1.00	1.00	0.99	1.00
54	1.9	1.25	0.65	0.21	218	1.00	0.98	2.42	1.00	0.71	1.00	1.00	0.96	1.00
55	1.9	1.12	0.78	0.34	172	1.02	0.80	11.1	1.38	0.20	1.00	1.01	0.55	1.00
60	1.8	1.31	0.49	0.04	209	1.00	0.99	1.05	1.00	0.98	1.00	1.00	1.00	1.00
61	1.8	1.07	0.73	0.29	281	1.02	0.85	9.80	1.26	0.24	1.00	1.01	0.65	1.00
62	1.7	1.25	0.45	0.00	195	1.00	0.99	1.02	1.00	0.99	1.00	1.00	1.00	1.00
63	1.7	1.23	0.47	0.13	474	1.00	0.97	1.98	1.00	0.79	1.00	1.00	0.97	1.00
64	1.6	1.15	0.45	0.00	208	1.00	0.99	1.02	1.00	0.99	1.00	1.00	1.00	1.00
65	1.6	1.13	0.47	0.03	622	1.00	0.99	1.13	1.00	0.97	1.00	1.00	0.99	1.00
67	1.5	1.06	0.44	0.00	706	1.00	0.99	1.09	1.00	0.98	1.00	1.00	1.00	1.00

5500 K, at $Z = 0.001$ larger than 6000 K. I.e., they would appear as evolved F or G type main sequence stars.

Important to unambiguously identify the stellar remnant of a supernova Ia progenitor system of the considered type is its peculiar surface chemical composition. These stars have peculiar abundances since they have lost a major part of their initial mass during the mass transfer phase, with the consequence that they uncover matter which has been sufficiently deep inside the star that thermonuclear reactions have occurred.. All main sequence stars in the present study in systems which lead to Type Ia supernovae lose at least $\sim 0.4\,M_\odot$, as the white dwarf needs to achieve the Chandrasekhar mass. However, in those systems where the white dwarf develops a wind the total mass loss of the main sequence stars may be considerably larger (cf. Tab. 5).

In a normal main sequence star, all isotopes of the light elements lithium, beryllium and boron are destroyed in the whole stellar interior except in an outer envelope of $\sim 0.1\,M_\odot$ (or $\sim 0.2\,M_\odot$ for boron). Therefore, the main sequence components of our systems are, at the time the supernova explosion occurs, all completely devoid of the light elements. The lack of these elements offers therefore already an unambiguous way to identify the remnant stars.

In Tab. 5, we compile other surface abundance anomalies found in our models. It can be seen, that the isotope ^{3}He is overabundant by a large factor, which is, however, hard if not impossible to verify observationally at the present time. The same may hold for other isotopic anomalies, e.g. of ^{13}C and ^{15}N. Only for carbon and nitrogen, we find the possibility of peculiar elemental abundances, i.e., carbon may be significantly underabundant and nitrogen correspondingly overabundant, as the CN-cycle is responsible for this feature.

The supernova explosion can in principle alter the abundances shown in Tab. 5 in two ways. It can lead to an additional mass loss of the main sequence star of the order of $0.1\,M_\odot ... 0.2\,M_\odot$ (Wheeler et al. 1975, Fryxell & Arnett 1981, Taam and Fryxell 1984). This may lead to a somewhat stronger CN-cycle signature but would not change our results qualitatively. It is further not excluded that it can lead to the deposition of small amounts of the supernova ejecta on the main sequence star (Fryxell & Arnett 1981, Taam and Fryxell 1984). Whether this happens or not seems to be unclear at the moment. In any case, the effect might be some enrichment of the surface composition of the main sequence star remnant with the nucleosynthesis products of the supernova, i.e. in elements between carbon and iron (Thielemann et al. 1986).

In summary, the light elements, e.g., lithium, and carbon are the most promising distinguishing chemical characteristics of main sequence type stellar remnants of Type Ia supernovae. Another independent characteristic may be a peculiar radial velocity or proper motion. The main sequence stellar remnants will at least have a peculiar velocity of the order of their orbital velocity at the time of the explosion of the white dwarf. This velocity is in the range $140\,\mathrm{km\,s^{-1}}...250\,\mathrm{km\,s^{-1}}$ for all our systems, with larger values corresponding to the low metallicity models. The momentum impacted by the supernova ejecta on the main sequence star may increase its space velocity up to as much as $\sim 500\,\mathrm{km\,s^{-1}}$ (Wheeler et al. 1975). Therefore, any main sequence type remnant star must have space velocities in a very favorable range. It is large enough to impose a clearly peculiar kinematic on the stellar remnant, but it is still much smaller than the velocity of the supernova ejecta, which implies that the star will remain for a long time close to the center of the supernova remnant. Chemical and kinematic signature together make it in fact a interesting project to search for a main sequence type stellar remnant in the gaseous remnant of the historical Galactic supernova 1006 (Wellstein et al. 1999b), which is very likely the product of an exploding white dwarf (Schaefer 1996).

6. Discussion and conclusions

We have studied the evolution of close binary systems consisting of a main sequence star and a white dwarf which are considered as candidates for progenitors of Type Ia supernovae. Based on an extended grid of models, we have studied the properties of the systems as a function of the initial donor star mass, initial white dwarf mass, initial period, and chemical composition.

Due to our numerical technique (Sect. 2) we obtain, for the first time, a complete picture of the time dependence of the mass transfer rate in such systems. We find that the mass transfer rate remains initially for about one thermal time scale of the main sequence star on a very low level during which nova outbursts are likely to occur. Then, the maximum mass transfer rate is rapidly reached, and most white dwarfs approach the Chandrasekhar mass during the decline phase of the mass transfer ($\ddot{M}_{\rm WD} < 0$; cf. Figs. 7 to 10). Our results will allow to investigate the effect of this time dependence of the mass transfer rate on the lower critical accretion rates for stationary nuclear burning on the white dwarf (cf. Sect. 2.1). This may be important, as Prialnik & Kovetz (1995) showed that these threshold values may be smaller for higher white dwarf temperatures. As for $\ddot{M}_{\rm WD} < 0$ the white dwarf temperature is expected to be higher at a given value of $\dot{M}_{\rm WD}$ compared to the case of $\ddot{M}_{\rm WD} = 0$, this effect may perhaps increase the parameter space of models which lead to Chandrasekhar mass white dwarfs.

In contrast to results based on simple estimates of the mass transfer rate (e.g., Eq. 12), we find that the rates increase strongly for lower initial white dwarf masses (Fig. 9). I.e., even systems with rather small initial white dwarf masses ($\sim 0.7\,\mathrm{M_\odot}$) can not be excluded to evolve to Type Ia supernovae. As Chandrasekhar mass white dwarfs are likely to rotate faster the smaller their initial mass is, this implies that rotation may be relevant in some Type Ia explosions (cf. Sect. 4.1).

We find that the mass transfer rates in low metallicity systems are, for the same initial main sequence star and white dwarf masses, much higher than at solar metallicity. I.e., the initial main sequence star mass range which results in good Type Ia supernova progenitor candidates shifts from $1.6\,\mathrm{M_\odot}...2.3\,\mathrm{M_\odot}$ to $1.4\,\mathrm{M_\odot}...1.8\,\mathrm{M_\odot}$ (Figs. 14 and 15). At low metallicity, this range is narrower, and supernova Ia progenitor systems need to have white dwarfs which are initially about $0.2\,\mathrm{M_\odot}$ more massive (see also Figs. 14 and 15), leading to a decrease of the Type Ia supernova rate with decreasing metallicity. We note that this effect differs from the wind inhibition effect proposed by Kobayashi et al. (1998).

It is of course tempting to speculate about effects of the metallicity dependence of the progenitor evolution on the supernova peak brightness or decline rate. However, although more realistic calculations of the white dwarf evolution to the Chandrasekhar mass are now possible, they need to be performed before definite conclusions can be drawn. This is so since, although the described effects are likely to introduce a Z-dependence to the supernova properties, it would interfere with other such effects as described by Höflich et al. (1998), Dominguez et al. (1999), and Umeda et al. (1999).

It is also hard to disentangle whether possible dependences of Type Ia supernova properties on their environment — as suggested by Branch et al. (1996) or Wang et al. (1997) — are due to the mentioned trends with metallicity or due to different progenitor types at work. The latter seems more likely considering the life times of our progenitor models (Tabs. 2 and 3). Although our low Z models invoke lower mass main sequence stars, their predicted life time is $< 1.5\,10^9\,\mathrm{yr}$, which is roughly similar for our solar metallicity models. I.e., Type Ia supernovae in elliptical galaxies, which may require progenitor life times of $10^{10}\,\mathrm{yr}$, can not be obtained from the type of model presented here, but may rather require scenarios with low mass red giant (Hachisu et al. 1996) or CO white dwarf (Iben & Tutukov 1984) donor stars.

We emphasize that, nevertheless, models of the considered type very likely exist in nature, as they correspond to the close binary supersoft X-ray sources (Kahabka & van den Heuvel 1997). The X-ray luminosities, periods, and main sequence star properties (Sect. 5.1 and Tab. 4) appear to agree quite well with observed systems. We also outline a way to test whether such systems can in fact evolve into Type Ia supernovae. We make unambiguous predictions for the chemical and kinematical properties of the stellar remnants of main sequence star + white dwarf systems after the explosion of the white dwarf (Sect. 5.2), which may be directly tested for the case of the historical galactic supernova 1006 (Wellstein et al. 1999b).

Acknowledgements. We are very grateful to Hans Ritter and Jochen Greiner for many helpful discussions. This work has been supported by the Deutsche Forschungsgemeinschaft through grants La 587/15 and 16 and, in part, by NASA Grant LSTA-98-022 and NASA Grant NAG5-3930.

References

Arnould M., Goriely S., Jorissen A., A&A 347, 572

Branch D., 1998, ARAA 36, 17

Braun H., 1997, PhD thesis, LMU München

de Kool M., Ritter H., 1993, A&A 267, 397

Dominguez I. Höflich P., Straniero O., Wheeler J.C. 1999, in: Nuclei in the Cosmos V, ed. N. Prantzos, (Paris: Editions Frontiers)

Eggleton P., 1983, ApJ 268, 368

Filippenko A.V., 1997, ARAA 35, 309

Fryxell B.A., Arnett W.D., 1981, ApJ 243, 994

Fujimoto M.Y., 1982, ApJ 257, 767

Greiner J., Hasinger G., Kahabka P., 1991, A&A 246, L17

Grevesse N., Sauval A.J., 1998, SSR 85, 161

Hachisu I., Kato M., Nomoto K., 1996, ApJ 470, L97

Hachisu I., Kato M., Nomoto K., Umeda H., 1999, ApJ 519, in press

Hamuy M. et al. 1996, AJ, 112, 2438

Heber U., Napiwotzki R., Reid I.N., 1997, A&A 323, 819

Höflich P., Khokhlov A., Wheeler J.C. 1995, ApJ, 444, 831

Höflich P., Khokhlov A. 1996, ApJ, 457, 500

Höflich P., Wheeler J.C., Thielemann F.K 1998, ApJ, 495, 617

Iben I. Jr., Tutukov A.V., ApJS 54, 335

Iglesias C.A., Rogers F.J. 1996, ApJ 464, 943

Kahabka P., van den Heuvel E.P.J., 1997, ARAA 35, 69

Kato M., Hachisu I., 1999, ApJL 513, L41

King A.R., van Teeseling A., 1998, A&A 338, 965

Kippenhahn R., 1974, ApSS 31, 117

Kippenhahn R., Weigert A., 1990, *Stellar structure and evolution*, Springer, Berlin

Kobayashi C., Tsujimoto T., Nomoto K., Hachisu I., Kato M., 1998 ApJ 503, L155

Koester D., Dreizler S., Weidemann V., Allard N.F., 1998, A&A 338, 617

Kolb U., Ritter H., 1992, A&A 254, 213

Kovetz A., Prialnik D., 1997, ApJ 477, 356

Lamers H.J.G.L.M., Cassinelli J., 1999, *Introduction to stellar winds*, Cambridge University Press, Cambridge

Langer N., 1998, A&A 329, 551

Langer N., Heger A., Wellstein S., Herwig F., 1999, A&A 346, L37

Li X.-D., van den Heuvel E.P.J., 1997, A&A 322, L9

Livio M., 1996, in *Evolutionary Processes in Binary stars*, R.A.M.J. Wijers et al., eds., Dordrecht, Kluwer, p. 141

Livio M., 1999, in *Type Ia Supernovae: Theory and Cosmology*, Cambridge Univ. Press, astro-ph/9903264

Livio M., Pringle J.E., 1998, ApJ 505, 339

Nauenberg M., 1972, ApJ 175, 417

Nomoto K., Sugimoto D., 1977, PASJ 29, 765

Nomoto K., Kondo Y. 1991, ApJ 367, L19

Nomoto K., Iwamoto K., Kishimoto N., 1997, Science 276, 1378

Papaloizou J., Pringle J.E., 1978, M.N.R.A.S. 182, 423

Perlmutter S. et al. 1999, ApJ, in press and astro-ph/9812473

Podsiadlowski Ph., Joss P.C., Hsu J.J.L., 1992, ApJ 391, 246

Prialnik D., Kovetz A., 1995, ApJ 445, 789

Provencal J.L., Shipman H.L., Hog E., Thejll P. 1998, ApJ 494, 759

Rappaport S.A., Di Stefano R., Smith M., 1994, ApJ 426, 692

Riess A.G., Press W.H., Kirshner R.P., 1995, ApJ 438, L17

Riess A., Filippenko A., Weidong L., Schmidt B. 1999, AJ, submitted & astro-ph/9907038

Ritter H., 1985, A&A 148, 207

Ritter H., 1988, A&A 202, 93

Ritter H., 1996, in *Evolutionary Processes in Binary Stars*, NATO ASI Ser. C, Vol. 477, eds., R.A.M.J. Wijers et al., Kluwer, Dordrecht, p. 223

Ritter H., Kolb U., 1998, A&AS 129, 83

Schaefer B.E., 1996, ApJ 459, 438

Schmidtke P.C., Cowley A.P., McGrath T.K., Hutchings J.B., Crampton D., 1996, AJ 111, 788

Sion E.M., 1999, PASP 111, 532

Taam R.E., Fryxell B.A., 1984, ApJ 279, 166

Thielemann F.-K., Nomoto K., Yokoi Y., 1986, A&A 158, 17

Umeda H., Nomoto K., Yamaoka H., Wanajo S., 1999, ApJ 513, 861

van Teeseling A., King A.R., 1998, A&A 338, 957

Verbunt F,. Zwaan C., 1981, A&A 100, L7

Wang L., Höflich P., Wheeler, J.C. 1997, ApJ 487, L29

Wellstein S., Langer N., 1999, A&A 350, 148

Wellstein S., Braun H., Langer N., 1999, A&A, in preparation

Wellstein S., Langer N., Gehren T., 1999b, A&A, in preparation

Wheeler C.J., Lecar M., McKee C.F., 1975, ApJ 200, 145

Wheeler C.J., 1996, in *Evolutionary Processes in Binary stars*, R.A.M.J. Wijers et al., eds., Dordrecht, Kluwer, p. 307

Woosley S.E., Weaver T.A., 1986, ARAA 24, 205